A MULTIPLE SOURCE DELIVERY SYSTEM FOR INTERSTITIAL LASER PHOTOCOAGULATION

A MULTIPLE-SOURCE DELIVERY SYSTEM FOR INTERSTITIAL LASER PHOTOCOAGULATION

By

DEIDRE L. BATCHELAR, B.Sc.

A Thesis

Submitted to the School of Graduate Studies

In Partial Fulfilment of the Requirements

for the Degree

Master of Science

McMaster University

MASTER OF SCIENCE (1996)
(Physics)

McMaster University
Hamilton, Ontario

TITLE: A Multiple-Source Delivery System for Interstitial Laser Photocoagulation

AUTHOR: Deidre L. Batchelar, B.Sc. (University of Western Ontario)

SUPERVISOR: Dr. Douglas R. Wyman

NUMBER OF PAGES: ix, 64

Abstract

Interstitial laser photocoagulation (ILP) is a minimally invasive technique for destroying solid, localised tumours thermally by delivering infrared laser energy directly into the targeted volume via percutaneously implanted optical fibres. Using current treatment parameters, each fibre delivers sufficient energy to destroy a volume of one to two cm^3; larger lesions may be created by using multiple fibres excited simultaneously. An efficient delivery system has been constructed consisting of several fibres bundled through a single cannula and splayed out through a specially designed tip. This delivery system is simple to use and provides accurate fibre placement.

By linearly superposing single source solutions to the bioheat transfer equation, a mathematical model for coalescent thermal lesions has been developed. It has been determined that large, clinically useful thermal lesions can be created by implanting four sources at the corners of a square. It has been demonstrated, through *ex vivo* experimentation in bovine liver, that the model correctly predicts the dimensions of the thermal lesions.

This work is dedicated to the memory of my grandfather, James Taylor.

Acknowledgements

I would like to thank my supervisor, Doug Wyman, for all his help and encouragement over the past two years. Thanks are also due to Tom Chow for keeping the lasers running and to John Blenky and Alan Hazelhurst in the machine shop at the Hamilton Regional Cancer Centre for constructing the delivery system. I have undying appreciation for Tamie Poepping and Deboleena Roy for all the discussions, pep talks and endless bottles of wine that got us all through last winter and for Heather Johanson who could always remind me that there was life beyond thesis. The Spicy Camel Dish Renovation Squad contributed greatly to maintaining my sanity in the final stages of this paper. Mum and Dad deserve a special mention for their support across the miles and finally - thanks to Jeremy Gill whose support helps me find perspective and who always inspires me. Thanks everybody!!!

Table of Contents

Table of Figures

Table of Tables

1. Introduction

1.1 Interstitial Laser Photocoagulation

1.1.1 General Description

Interstitial laser photocoagulation (ILP) is a minimally invasive technique for killing solid, localised tumours thermally. This is accomplished by delivering infrared, or near infrared, laser energy directly into the target volume via percutaneously implanted optical fibres. Sufficient energy is delivered in this manner to raise the local temperature beyond the threshold for protein denaturation, 60°C. Tumour cells subjected to this thermal stress undergo immediate thermal coagulative necrosis.

1.1.2 Historical Perspective

The healing potential of heat has been known for centuries. The first reference to the use of heat to destroy tumours is found in *The Edwin Smith Surgical Papyrus,* dating from 1700 BC, which described the use of a firedrill to treat breast tumours (Breasted, 1930). Modern use of thermal action as a therapy for cancer has its roots in an observation made by Busch in 1866 (Busch, 1866). He noted that a facial sarcoma was completely eradicated in a patient who had suffered two attacks of erysipelas, an infection accompanied by a 40°C fever. This discovery encouraged physicians to attempt to treat cancer by deliberately inducing pyrexial states in patients. By injecting cancer patients

with a filtrate of cultured *Streptococcus pyogenes* and *Bacillus prodigiosus* to induce temperatures of 41°C for several hours, Coley, in 1893, demonstrated that deliberate hyperthermia leads to the regression, and in some instances the cure, of sarcomas (Coley, 1893).

The development of thermal action as a viable therapeutic modality was restricted in the first half of the 20th century. Not only was there a lack of knowledge of the mechanisms by which heat destroyed cells but also an inability to sufficiently localise the application of thermal energy. Treatments such as Coley's, where the whole body temperature of the patient was raised for several hours, risked patients' lives. An alternative mode of therapy, where the affected organ was heated, was only effective for surface tumours and risked widespread damage to the target organ. Research at this time was limited to determining the effect of thermal action on tissues of differing histological characteristics.

Bown, in 1983, was the first to describe the use of interstitially directed laser energy as a source of thermal energy for the destruction of unresectable tumours (Bown, 1983). This approach can be applied to conventional hyperthermia by supplying laser power of approximately 1W for greater than an hour (ILH). This raises the local temperature to between 42°C and 45°C causing irreversible damage to the cells and resulting in cell death at a later stage in the cell cycle (Hall, 1988). A novel use of thermal energy to destroy tissue arose using interstitially applied laser energy. For interstitial laser photocoagulation, powers between 1.5W and 2.5W (Amin, Donald *et al.*, 1993; Wyman, Whelan and Wilson, 1992) are applied for approximately

1000 s, raising the temperature of surrounding cells above 60°C, thereby inducing immediate coagulative necrosis (Thomsen, 1990). Not only does ILP reduce therapy duration but, due to the immediate nature of the cell death, ILP can be guided and monitored by radiologic imaging techniques (Malone, Wyman, DeNardi, *et al.,* 1994; Nolsøe *et al.,* 1993; Amin, Donald, *et al.,* 1993; Bleier *et al.,* 1991; Schrottner *et al.,* 1990). Since its inception many studies at the biophysical and preclinical levels have been performed to determine optimal delivery parameters, safety and efficacy (Whelan *et al.,* 1995; Malone, Lesiuk, *et al.,* 1997; Wyman, Wilson, Adams, 1994; Schatz *et al.,* 1992; Dachman *et al.,* 1990; Matthewson *et al.,* 1989). Before the appropriate clinical use of ILP can be determined it is necessary to further our knowledge in these three areas as well as determining the best methods for imaging control of the technique.

1.2 Laser Tissue Interactions

1.2.1 Initial Energy Deposition

For radiation in the visible or near-infrared regions of the spectrum, the primary cause of damage is thermal effects (Thomsen, 1990; Hillenkamp, 1980). When tissue is exposed to light, the radiation is transmitted, scattered or absorbed in proportions dependant upon the wavelength of light and the optical properties of the tissue (Welch, 1984). For near infrared wavelengths the dominant interaction is light scattering and the radiation may travel several millimetres before being absorbed (Jacques *et al.,* 1992; McKenzie, 1990;

Frank, 1989;). Multiple scattering in this region of the spectrum tends to produce a uniform distribution of light in the tissue. The main chromophores, or absorption centres, for visible radiation (400nm to 1000nm) are haemoglobin, the oxygen transportation molecule in red blood cells, and melanin, a pigment found in skin and the retina. Above 1000nm, in the infrared region, all biomolecules have specific and strong vibrational absorption bands (Jacques *et al.,* 1992; Frank, 1989; Hillenkamp, 1980).

For ILP using a plane cut optical fibre, the fibre tip approximates a point optical source. Upon absorption, the optical energy is transformed into a diffuse heat source and tissue damage is caused by subsequent thermal effects, such as thermal coagulative necrosis and hyperthermic cell killing.(Amin, Buonaccorsi, *et al.,* 1993; Wyman *et al.,* 1992; Thomsen, 1990)

1.2.2 Biological Damage

During ILP, exposed tissues undergo a sequence of thermally induced changes leading to irreversible damage (Prapavat *et al.,* 1996; Thomsen, 1990; Pearce, 1990). This damage is well described by the same Arrhenius rate kinetics as first order chemical reactions (Agah *et al.,* 1994; Birngruber , 1980; Pearce and Thomsen, 1993). The damage induced depends on the entire time-temperature history of the tissue. For example, the threshold for instantaneous protein denaturation is, typically, 60°C but proteins will become denatured when exposed to lower temperatures for longer periods (Beacco *et al.,* 1994; Thomsen, 1990; McKenzie, 1990). As the laser tissue interaction depends on the absorption and scattering properties of the exposed tissue, the tissue

response to laser excitation depends on both the degree and nature of previously acquired damage. ILP is, thus, a non-linear process.

Visual observation of an ILP lesion immediately following irradiation provides a map of thermal damage to soft tissue. In an optically dense tissue, such as liver, the thermal lesion will appear as a series of concentric rings. The centre is a small hollow region resulting from vaporisation. This is surrounded by a ring of carbonised and caramelised tissue that is, in turn, enclosed in a larger zone of coagulation. A ring of haemorrhage or edema may circumscribe the lesion.

1.2.2.1 Thermal Coagulation

The hallmark of ILP is the immediate appearance of coagulative necrosis when local temperatures are raised above the commonly assumed threshold of 60°C. This coagulation is due to the denaturation of structural proteins (Thomsen, 1990; Pearce, 1990; Hillenkamp, 1980). In their native state, one or more protein chains will be arranged together in structures of high spatial order known as their conformation (Raven and Johnson, 1986). The most abundant structural protein is collagen which forms a triple helix structure.

Conformations are stabilised by hydrogen and van der Waal's bonds with binding energies of only 0.04 eV to 0.4 eV. Any heating above normal physiological temperatures will excite these biomolecules into higher vibrational states and cause the weak bonds to break with a resulting loss of conformation, i.e., the protein will become denatured (Hillenkamp, 1980). The

loss of structure is accompanied by a loss of function because most biochemical reactions require the reactants to be closely matched structurally.

1.2.2.2 Water Vaporisation

Most soft tissues are approximately 80% water, so, as temperatures approach 100°C, water vaporisation becomes the dominant photothermal process. As intracellular water heats up it expands, with or without phase change, and this contributes to the stress applied to the tissue. The steam formed by evaporation collects in extracellular vacuoles. As the vapour pressure begins to increase the vacuoles coalesce and grow larger. Eventually the pressure will become great enough that the walls of the vacuole will rupture explosively, an event known as the "popcorn effect"(Hillenkamp, 1980; Thomsen, 1990; Pearce, 1990). Fragmentation of large tissue pieces may be caused by these explosions.

1.2.2.3 Tissue Ablation

Once the tissue is completely desiccated, further energy deposition results in removal of tissue mass by ablative processes such as tissue carbonisation and fragment ejection. As temperatures continue to increase, the tissue is broken down thermally into smaller and smaller pieces until it is reduced to small chain hydrocarbons, CO, CO_2 or elemental carbon. This results in a residue of black char accompanied by the production of a grey smoke.

Photothermal Effects	Approximate Temperature of Onset	Histopathologic Effect
damage accumulation processes	37°-43° 45°-60° 60°-100°	reversible damage deactivation of enzymes, edema photocoagulation
water-dominated processes	100°+	desiccation, water vaporisation, extracellular vacuole formation, "popcorn" effect
high temperature processes	300°-1000° 3550°	tissue ablation vaporisation of carbon

Table 1.1: Summary of thermal laser–tissue bioeffects

1.3 Clinical Status of ILP

ILP remains an experimental therapeutic technique. Clinically, it has been used to kill unresectable, solid tumours in the brain (Roux *et al.,* 1992; Schrottner *et al.*, 1990), head and neck (Ohyama *et al.,* 1988; Castro *et al.,* 1992), liver (Steger *et al.,* 1989; Dowlatshahi *et al.*, 1991; Hahl *et al.,* 1990; Masters *et al.,* 1991), and breast (Harries *et al.,* 1994). Approximately ¾ of the patients who have undergone ILP treatment received it as palliative care for colorectal metastases in liver. Potential hazards involved in ILP therapy have been studied in both animal models and during clinical applications (Malone *et al.,* 1994; Steger, Lees, *et al.,* 1992; Amin, Donald, *et al.,* 1993; Dachman *et*

al., 1990; Schatz *et al.,* 1992; Malone, Lesiuk, *et al.,* 1997; Amin, Bown and Lees, 1993; Wyman, Schatz and Maguire, (in press)).

ILP can be used as an alternative to percutaneous alcohol injection, cryotherapy or brachytherapy in the liver (Masters *et al.,* 1991; Dowlatshahi *et al.,* 1992; Malone *et al.,* 1994), and stereotactic radiosurgery or brachytherapy in the brain. ILP does not require the introduction of drug or the use of ionising radiation. A further advantage of ILP over other modalities is that tumour cells are destroyed immediately. This allows for visualisation of the lesion using real-time ultrasound (Malone *et al.,* 1992; Dachman *et al.,* 1990; Amin, Donald *et al.,* 1993; Harries *et al.,* 1994; Malone, Lesiuk *et al.,* (in press)) or magnetic resonance imaging (Schrottner *et al.,* 1990; Bleier *et al.,* 1991; Roux *et al.,* 1992) and opens the possibility of using an imaging feedback system to control the treatment. The immediacy of cellular destruction also allows for more precise control of the destroyed volume by careful manipulation of the exposure parameters.

1.4 Delivering ILP

Traditionally it has been assumed that there is a positive correlation between optical penetration of tissue and coagulative necrosis volume. Thus Nd:YAG lasers operating at 1064 nm have been considered to be the most suitable energy source for ILP because this wavelength is maximally penetrative in soft tissue. (Svaasand, 1989; Jacques *et al.,* 1992; Svaasand *et al.,* 1990) However, recent experience has shown that, for equivalent power and exposure duration, point heat sources result in larger coagulative lesions (Amin,

Buonaccorsi, *et al.,* 1993; Wyman *et al.,* 1992) than do point optical sources. In spite of this, lasers still remain the energy source of choice for percutaneous thermal therapy. Lasers are capable of delivering a precise and predictable amount of energy to the target. The energy is delivered by means of optical fibres which offer the advantage of being narrow, flexible, non-ferrous and providing efficient energy coupling.

It is possible for the implanted optical fibres to function as point heat sources. As thermal damage is accumulated in the tissue, the properties of the tissue change and the optical penetration of any wavelength is decreased. When tissue temperatures exceed the charring threshold, the optical penetration is decreased to the extent that the energy is entirely deposited within the char at the fibre tip and the source essentially becomes a point heat source. (Wyman *et al.,* 1994) This process may be accelerated by seeding a speck of char on the distal tip of the optical fibre causing the fibre to act as a point heat source immediately. Precharring the tip also leads to more consistent volumes of thermal necrosis (Amin, Buonaccorsi, *et al.,* 1993). Thus, ILP may be performed as well or better using wavelengths that are absorbed in tissue more effectively than 1064 nm Nd:YAG radiation.

This suggests the possibility of applying laser diodes operating in the region of 800 nm to ILP. These lasers offer considerable practical advantages. They are relatively inexpensive, can use standard electrical outlets, require no warm-up time, need only be air cooled, are small and easily portable. Optical energy around 800 nm has a higher absorption coefficient than 1064 nm leading to a quicker conversion to a point heat source. Several studies have

indicated that these lasers are potentially the most appropriate energy source for ILP. (Prapavat *et al.,* 1996; Jacques *et al.,* 1992)

Although it has been clearly demonstrated that a point heat source can be used to create larger thermal lesions, some caution must be exercised. Tissues are more likely to char when subjected to point heat irradiation than point optical. This is accompanied by increased smoke and vapour production. The location of the tumour and the monitoring technique used determine whether vaporisation is acceptable or not. It is thought that the hyperechoic ultrasound images used to monitor hepatic ILP arise from microbubbles produced by vaporisation (Malone *et al.,* 1994). There are, however, cases where it may be clinically relevant to question if sizeable charring and vapour production can be avoided. In animal studies, it has been seen that it is possible for vapour produced in the brain to be transported through the ventricular system to cause damage to the ependymal lining. (Wyman, Schatz and Maguire, (in press)) This is an unacceptable clinical risk.

It is possible to avoid charring by directly cooling the tip of the fibre (Dowlatshahi *et al.,* 1992; Hahl *et al.,* 1990) or by using fibres with diffusing tips to reduce the local power density (Panjehpur *et al.,* 1990; Nolsøe *et al.,* 1992; Prapavat *et al.,* 1996; van Hillegersberg *et al.,* 1994; Dowden *et al.,* 1987). These systems have been shown to be capable of producing single fibre lesions with diameters of 1.0 cm in 600s for powers greater than 3.0W. This indicates that the technique can be adapted for use at sites where charring and vaporisation are not clinically permitted.

In the interest of practicality, it may be best to limit the use of cooled or diffusing tips to locations where they are required. These systems require additional technology resulting in additional expense. The diffuser tips are single use only, have poor structural integrity (Malone *et al.*, 1992) and are unusable if the tip is damaged. A fibre that is plane cut and uncovered is reusable and if the tip is damaged it is easily reparable even during therapy preparation.

1.5 Scope of the Project

Using standard delivery parameters a single fibre illumination can result in no more than 1-2 cm^3 of coagulative necrosis. This is insufficient to eradicate many hepatic tumour nodules. In order for ILP to be a viable therapeutic modality it is necessary to develop methods of enlarging the thermal lesion volume. One straightforward method of accomplishing this is to irradiate the sample with several sources simultaneously. If the sources are placed sufficiently close together the temperature fields from each will overlap. This will result in temperature elevations greater than either source could produce individually and, hence, a coagulation volume greater than the sum of individual volumes. It has been suggested that an arrangement consisting of four coplanar fibres implanted on the corners of a square would be an effective treatment mode (Steger, Lees, *et al.,* 1992; Davis *et al.,* 1988; Steger, Shorovon, *et al.,* 1992; Masters *et al.,* 1991). This would provide a large area of coagulation in the plane defined by the sources. The fibres could then be retracted along the implantation axis and the irradiation repeated to further

enlarge the lesion(Steger *et al.,* 1989). Tests using this form of array have been carried out both in animals and in humans.

Treatment set up for multiple fibre irradiations has involved implanting each fibre individually under ultrasound guidance. This is time consuming and does not easily provide for accurate relative positioning of the sources. Steger, Lees *et al.* (1992) describe a template consisting of four screw collets set into a plastic disk. The fibres were set into the collets and the screws were tightened to prevent movement along the line of the fibre. Once all four fibres were positioned at the proper penetration depth, the entire array was inserted percutaneously into the liver. Different source separations were achieved by use of disks of varying dimensions. This improves the control of relative positioning but does not streamline the process. In addition, having a separate injection site for each fibre increases the risk of infection to the patient. Source separations are, at present, determined empirically by varying the treatment settings and fibre spacing, monitoring the lesion formation, then looking for overlapping lesions post-mortem. Steger, Lees *et al.* (1992) found only a 75% chance of creating coalescent lesions using this method. Although the temperature fields and potential treatment volumes have been calculated around four fibres in a square (Davis *et al.,* 1988), the problem of determining the optimal arrangement of four fibres for a given set of irradiation parameters has not been examined. The problem of selecting optimal source locations for two sources has been solved (Wyman, 1993).

The aim of this work is to refine the use of multiple source ILP. This will be accomplished by demonstrating that it is possible to predict the optimal

separation of fibres mathematically and that this can be used to design a single cannula capable of delivering all four fibres through one injection site. It will be shown that such a delivery system can be constructed on site from readily available materials. The device will be tested in *ex vivo* bovine liver for ease of use, accuracy of fibre placement and reproducibility of lesion size. The dimensions of the lesions produced will be compared to those predicted by the model. This sort of predictive modelling provides the first step towards full treatment planning for ILP treatment of hepatic tumours.

2. Mathematical Modelling

The primary goal of this study is to assess the feasibility of using a single cannula to deliver four optical fibres for hepatic ILP therapy. The mathematical modelling of this problem is, therefore, directed towards determining the optimal separation of a set of thermal sources and predicting the gross dimensions of the lesions produced.

2.1 Steady-State Temperature Response

If the ILP treatment period is longer than the time required for the temperature distribution to reach equilibrium it is possible to use a steady-state model to predict the volume of damage incurred during an irradiation. For ILP using only one fibre, temperatures are near steady-state by the end of a 500s irradiation (Malone *et al.,* 1992; van Hillegersberg *et al.,* 1994; Wyman and Whelan, 1994). Davis, Dowden *et al.* (1989) have indicated that it should be possible to evaluate the performance of a four fibre arrangement using a steady-state formulation.

The starting point for a mathematical assessment of thermal damage to tissue is the bioheat transfer equation. For an infinite homogeneous medium this can be expressed as

$$\rho c \frac{\partial T}{\partial t} = k_{eff} \nabla^2 T(r,t) + P(r,t) \tag{2.1}$$

where T (K) is the increase in temperature, ρ (g/cm^3) is the density of the material, c (J/g/K) is the heat capacity, k_{eff} (W/cm/K) is the effective thermal conductivity and P (W/cm^3) is the heat source. The thermal conductivity is referred to as effective because it combines thermal conduction and blood perfusion cooling in one term following the Weinbaum-Jiji heat transfer model (Weinbaum and Jiji, 1985). There is no consensus on what is the most effective way of dealing with blood perfusion cooling and many different models have been proposed (Arkin *et al.,* 1994). The effective thermal conductivity approximation was chosen for its simplicity. Equation (2.1) is also approximate because it does not account for spatiotemporal variations in the tissue properties arising during heating.

The temperature response of tissue to a thermal insult can be obtained by solving equation (2.1) using Green's functions as demonstrated by Vyas and Rustgi, 1992. At steady-state the solution for a steady point heat source of unit power is the Green's function (Carslaw and Jaeger, 1989)

$$T_G(|r - r'|) = \frac{1}{4\pi\ k_{eff}|r - r'|} \tag{2.2}$$

When the point heat source emits a total power of P_T, the temperature response is simply

$$T(r) = \frac{P_T}{4\pi\ k_{eff}\ r} \tag{2.3}$$

where r is the distance from the source.

It is possible to simplify the model by rewriting equation (2.3) in terms that can be obtained through simple experiments. The temperature at the end of the time-temperature history of a thermal lesion at which coagulation is observed is referred to as the coagulation temperature, T_c. The coagulation radius from a single source may be denoted by r_c so that $T(r_c) = T_c$, the coagulation temperature. Thus the temperature response may be expressed as

$$T(r) = \frac{T_c}{r/r_c} \tag{2.4}$$

where

$$T_c = \frac{P_T}{4\pi\ k_{eff} r_c} \tag{2.5}$$

is the steady state temperature increase at the coagulation radius, r_c.

For the lesion produced by four sources in a square, the contributions from each source must sum to be T_c on the boundary

$$2\frac{T_c}{r/r_c}+2\frac{T_c}{r_w/r_c}=T_c \tag{2.6}$$

where

$$r_w=\sqrt{\left(\frac{d}{2}\right)^2+\left(\frac{w}{2}\right)^2}\ and\ r=\sqrt{\left(\frac{d}{2}\right)^2+\left(d+\frac{w}{2}\right)^2}\ . \tag{2.7}$$

Figure 2.1 illustrates the geometry used to determine the optimal source separation as well as the treatment area defined as useful given by

$$A=(d+w)^2 \tag{2.8}$$

This area will be optimised to determine the appropriate source separation. It is legitimate to limit the optimisation to two dimensions. In practice large volumes of tissue will be destroyed by irradiating, retracting the fibres and re-irradiating (Steger *et al.,* 1989) to create stacks of lesions. It is, therefore, useful to ensure that the size of each lesion is maximised in the plane perpendicular to the line of retraction.

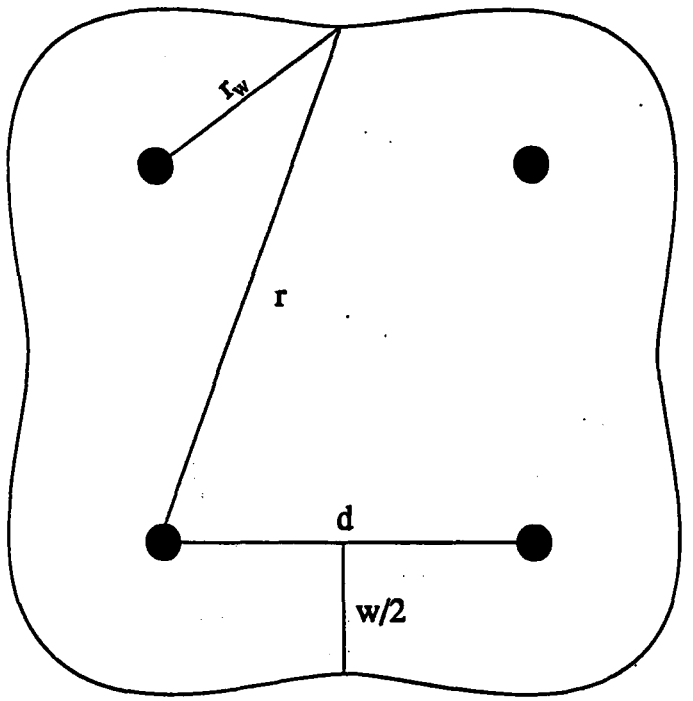

Figure 2.1: The geometry of the mathematical model

The optimisation problem was solved using the method of Lagrange multipliers

$$\frac{\partial A}{\partial d} = \lambda \frac{\partial f}{\partial d}$$

$$\frac{\partial A}{\partial w} = \lambda \frac{\partial f}{\partial w} \qquad (2.9)$$

$$f(d,w) = 0$$

where the equation of constraint, f(d,w)=0, is a re-arrangement of equation (2.6)

$$f(d,w)=\left(\left(\frac{d}{2}\right)^2+\left(\frac{w}{2}\right)^2\right)^{-\frac{1}{2}}+\left(\left(\frac{d}{2}\right)^2+\left(d+\frac{w}{2}\right)^2\right)^{-\frac{1}{2}}-1/2r_c=0 \qquad (2.10)$$

The bulk of this problem is straightforward and can be solved analytically. Since $\frac{\partial A}{\partial d}=\frac{\partial A}{\partial w}=2(d+w)$, d and w can be solved for by equating the two partial derivatives of equation (2.10). After some algebraic manipulation, and defining dimensionless α as the ratio w/d, the problem is reduced to

$$(\alpha^2+4\alpha+5)^3(\alpha-1)^2-(\alpha^2+1)^3(\alpha+3)^2=0 \qquad (2.11)$$

Knowing that α has to be positive, the appropriate solution to (2.11) was calculated using Newton's method to be α=1.59. The exact values of d and w were then determined by rearranging equation (2.10) to obtain

$$d=4r_c\left[\frac{1}{\sqrt{1+\alpha^2}}+\frac{1}{\sqrt{1+(2+\alpha)^2}}\right] \qquad (2.12)$$

Thus the optimal separation for four sources at the corners of a square and at steady-state is $d=3.21r_c$ and $w=5.09r_c$. Only knowledge of the coagulation radius, r_c, is needed to determine the exact distance required. This was easily

determined experimentally for any delivery parameters by performing single-source irradiations.

Before proceeding with experiments, the lesion shape for fibres set at the optimal separation was calculated. This was done to confirm that the four-fibre arrangement would produce a clinically relevant lesion; one with "reasonably" flat, convex boundaries. The temperature increase due to each of the sources is described by equation (2.4) and, at the lesion boundary, the contributions from each source must sum to be T_c. Equation (2.13) expresses this relationship where r_i is the distance from the ith source to the point on the boundary under consideration.

$$\sum_{1}^{4} \frac{1}{r_i} - \frac{1}{r_c} = 0 \qquad (2.13)$$

Newton's method was used to determine the z-value for each x-y point in the lesion plane. This problem was coded in Interactive Data Language (IDL), a high-level array-oriented programming language. The source code may be found in the appendix.

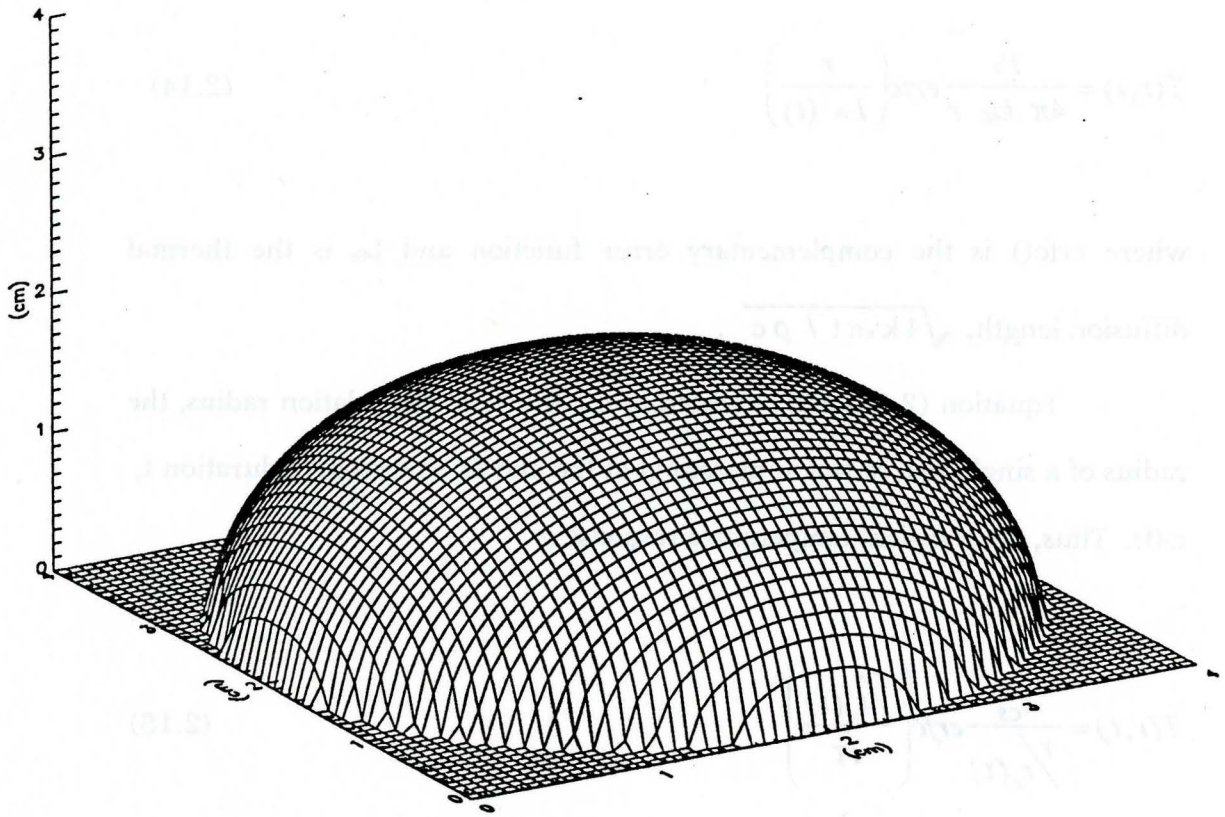

Figure 2.2: Predicted lesion boundary in half-space above plane containing four 1.2W, 600 s sources at steady-state.

2.2 Transient Temperature Response

Early experimental results indicated that the steady-state description of the tissue temperature response was inadequate (see Chapter 4). To rectify this a transient model was invoked. The procedure in this case parallels that of steady-state. The solution to equation (2.1) in the case of a transient response

to a steady, isotropic point thermal source of power P_T is (Wyman and Whelan, 1994)

$$T(r,t) = \frac{P_T}{4\pi\ k_{eff}\ r} erfc\left(\frac{r}{L_{th}\ (t)}\right) \tag{2.14}$$

where erfc() is the complementary error function and L_{th} is the thermal diffusion length, $\sqrt{4\,k_{eff}\,t\ /\ \rho\,c}$.

Equation (2.14) can be scaled to the transient coagulation radius, the radius of a single source lesion measured at the end of an exposure duration t, $r_c(t)$. Thus, the transient temperature response is

$$T(r,t) = \frac{T_{CS}}{r/r_c(t)} erfc\left(\frac{r/r_c(t)}{\sqrt{\tau}}\right) \tag{2.15}$$

where

$$T_{CS} = \frac{P_T}{4\pi\ k_{eff}\ r_c(t)} \tag{2.16}$$

is the steady-state coagulation temperature which results in a lesion dimension of $r_c(t)$ and τ is a dimensionless time, given by

$$\tau = \left(\frac{L_{th}(t)}{r_c(t)} \right)^2 \tag{2.17}$$

Again, the area illustrated in figure 2.1 is optimised using Lagrange multipliers. This time the equation of constraint is obtained by summing the contributions from each source to be the transient coagulation temperature, $T(r_c(t))=T_c(\tau)$, on the boundary so that

$$f(d,w) = \frac{erfc\left(r / r_c(t)\sqrt{\tau} \right)}{r} + \frac{erfc\left(r_w / r_c(t)\sqrt{\tau} \right)}{r_w} - \frac{erfc\left(1/\sqrt{\tau} \right)}{2r_c(t)} = 0 \tag{2.18}$$

where r and r_w are as given in equation (2.7). The transient optimisation was accomplished by determining the radius of coagulation and dimensionless time for each set of delivery parameters and then solving for d and w numerically. The IDL code for this may be found in appendix. Once d and w were obtained, the predicted lesion shape was determined by inputting the appropriate function

$$\sum_{1}^{4} \frac{erfc\left(r_i / r_c(t)\sqrt{\tau} \right)}{r_i} - \frac{erfc\left(1/\sqrt{\tau} \right)}{r_c(t)} = 0 \tag{2.19}$$

to the code written for the steady-state situation (appendix).

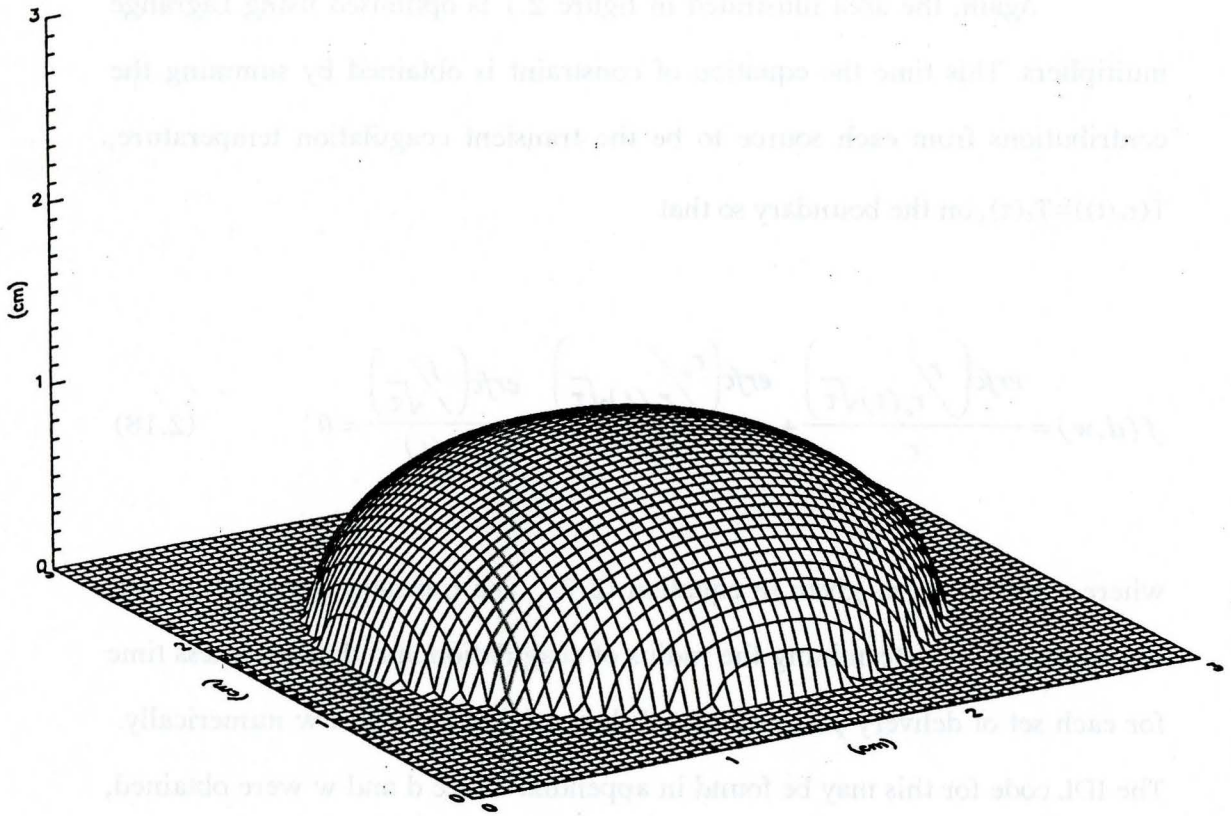

Figure 2.3: Predicted lesion boundary in the half-space above plane containing four 1.2 W, 600s sources, for a transient temperature response. Note that the lesion is smaller than the lesion produced by the same sources operating under steady-state conditions. This is due to the more rapid temperature fall off of the transient response.

3. Materials and Methods

3.1 Design and Construction of the Splay-tip Cannula

To minimise both the financial and time expenditure, the design of the multiple source delivery cannula had to be simple enough that it could be constructed in an on-site machine shop and the materials used must be readily available and reasonably inexpensive. The materials should also have melting points higher than the temperatures reached within the lesion as it will not be possible to retract the cannula once the fibres are in place. Temperatures can exceed 300°C at the centre of the lesion (Prapavat *et al.,* 1996). In addition, the tip must allow for easy loading and extruding of the fibres without breakage.

The apparatus designed for this study consisted of a hollow aluminum cannula with a screw-on tip. The tip has four channels carved through it, set at 20° to the central axis of the cannula. The fibres are passed through the tube and inserted into the channels. The tube is then screwed on to the tip. The channels are long enough to secure the fibres in place during insertion. The friction of the fibres against one another at the entrance apertures is sufficient to prevent movement back along the line of the fibre during irradiation.

The diameter of this system has a lower bound determined by the core diameter of the optical fibres to be used. Two cannulae have been constructed

at the Hamilton Regional Cancer Centre to demonstrate the size advantage gained by using fibres with smaller diameters. A cannula designed to admit 200μm fibres is 3mm in diameter while one for use with 400μm is 5mm (figure 3.1). The 3mm cannula represents the lower limit of what could be machined in our shop. The 5mm cannula is used for all testing reported here because the diode lasers used were coupled to 400μm fibres during manufacturing.

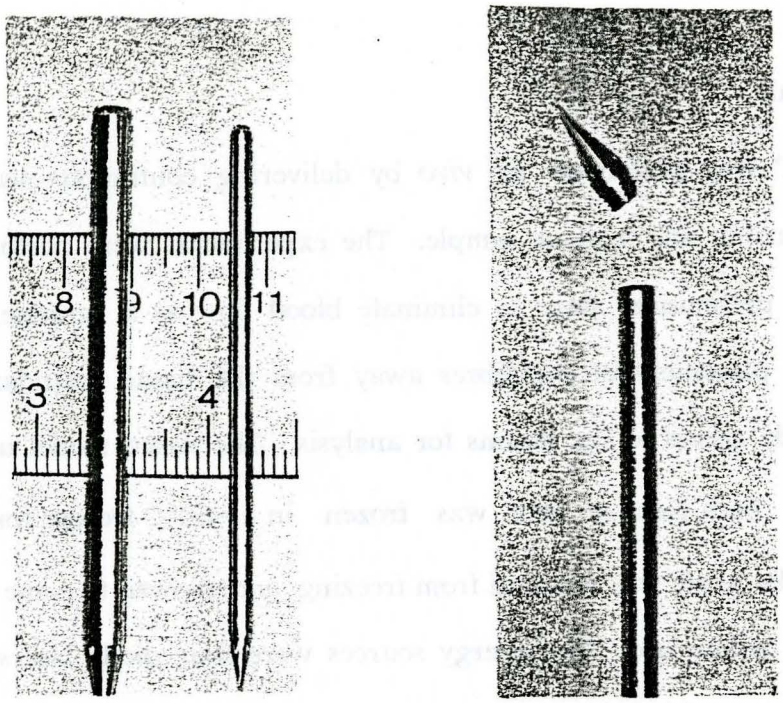

a b

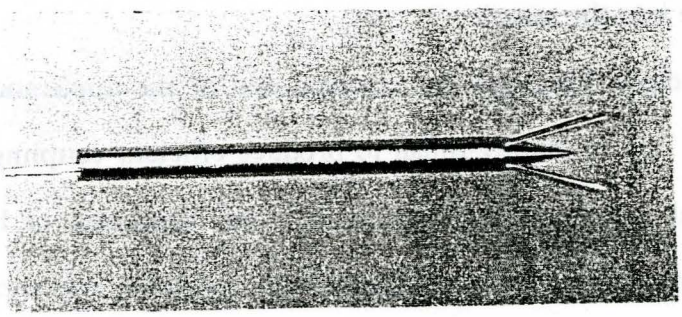

c

Figure 3.1: The multiple source delivery system consists of (a) cannula (two are shown), (b) a screw-on tip and (c) extruding fibres.

3.2 Materials

ILP was performed *ex vivo* by delivering continuous-wave laser radiation directly into a tissue sample. The experiments were performed *ex vivo* at this preliminary stage to eliminate blood flow as a variable, and to enable easy placement of the fibres away from the tissue boundaries and provide ready access to the lesions for analysis. The tissue model used was bovine liver. Each piece of liver was frozen in a –80°C freezer for at least 24 hours. The tissue was removed from freezing and allowed to come to room temperature before use. The energy sources were four diode lasers (model LDP-4380C, Laser Diode Inc., NJ) operating at 805nm. The energy from each was delivered through two sequential, coupled 400μm core diameter quartz optical fibres. One end of the diode fibre is connected directly to the diode. The other end is coupled to the application fibre, which guides the radiation from the diode fibre into the sample.

The diode fibre and the coupled end of the application fibre were polished to an optical quality finish to produce efficient coupling and prevent damaging back reflection into the diode. The condition of both tips was checked periodically during experimentation. Polishing was repeated for any sign of diminished surface quality on the fibre. After polishing, each application fibre was fixed in a chuck and mounted in front of a diode fibre. Coupling of the diode and application fibre was accomplished by directly abutting the two. Immediately prior to each irradiation, the output power was calibrated using a laser power meter (Ophir model DG, Jerusalem) accurate to ±0.01W.

The application end of the application fibre was blunt cut and rough polished using 600 grade sandpaper before each use. There was no need to perform a higher grade polish on this end because using an absorptive wavelength in a chromophore rich medium like liver leads to char induction at the fibre tip within seconds (Jacques *et al.,* 1992). There are also indications that unpolished fibres facilitate char formation (Wyman, Wilson and Adams, 1994). For each irradiation the fibre jacket and cladding at the distal fibre end were stripped back by 4.1 cm. This great length was exposed because the four fibre cannula requires several centimetres of bare fibre for the fibres to fit in the cannula tip. The exact length was chosen because there was a permanent groove on the fibre stripper at this point, allowing for easy reproduction of the stripped length.

3.3 Experimental Protocol

Two sets of experiments were performed. The single fibre irradiations were conducted to determine appropriate power-time settings to enable thorough testing of the four fibre model using the new cannula.

3.3.1 Single Fibre Irradiations

Irradiations were performed at a range of power-time settings.

Delivered Power (W)	Time (s)	Number of Irradiations
1.2	600	10
	1200	3
1.1	600	2
1.0	600	2
	720	2
	840	2
	960	2
	1080	2
	1200	2
0.9	600	10
	1200	5

Table 3.1: Summary of the *ex vivo,* single fibre irradiations performed varying the delivered power and exposure duration

For each, the laser output was adjusted to the required power. The application fibre was then inserted approximately 1.5cm into the sample through the surface of the liver. This simulated percutaneous implantation. The laser was switched on and the sample was irradiated for the duration of interest. Four irradiations were carried out simultaneously.

After the laser was turned off, the sample, consisting of a block of liver approximately 5 cm per side, was cut open to expose the induced lesion. The slice was made as close to the centre of the lesion as possible. This was accomplished by cutting along the line of the fibre while it was still implanted. It was possible to cut closely to the centre of the char in roughly 50% of the lesions. In the other cases more than one slice was required. Once the lesion was dissected, the diameter was measured. When a single cut was sufficient to expose the mid-plane of the lesion, both sides of the lesion were measured. For some settings the lesions produced were elongated along the fibre. Both axes were measured and averaged in these instances.

3.3.2 Multiple Fibre Irradiations

From the single fibre irradiations, three power-time settings were chosen for multiple fibre testing; 1.2W for 600s and 0.9W for 600 and 1200s. The optimal separation was determined for each coagulation radius. This was converted to an extension distance by applying simple trigonometry.

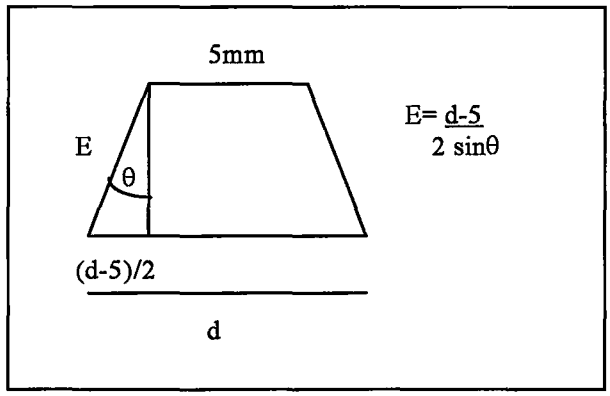

Figure 3.2: Determining the fibre extension, E, required to provide an inter-source separation of d when $\theta=11.5°$ and the separation between exit apertures in the cannula tip is 5 mm.

Five irradiations were performed at each set of parameters. For each irradiation the fibres were blunt cut, rough polished and the laser calibrated immediately before loading into the multiple source cannula. The cannula was injected approximately 2 cm into a large block of liver and each fibre was extruded the requisite distance by hand. The insertion depth of the fibres was guided by marks painted on the fibre jacket.

Post-irradiation, the lesion was exposed by first cutting perpendicular to the plane containing the sources (the char plane) along the channel created by the cannula. Once the characteristic whitening of coagulation was revealed,

slices were made parallel to the plane until the midline of the lesion was exposed. Twenty measurements were taken of each lesion as illustrated in figure 3.3. All of these were used to establish the reproducibility of the coagulated volume. The dimensions G and H were used to establish agreement between the model and experiment while the inter-char spacing, measures M through P, verified the source separations.

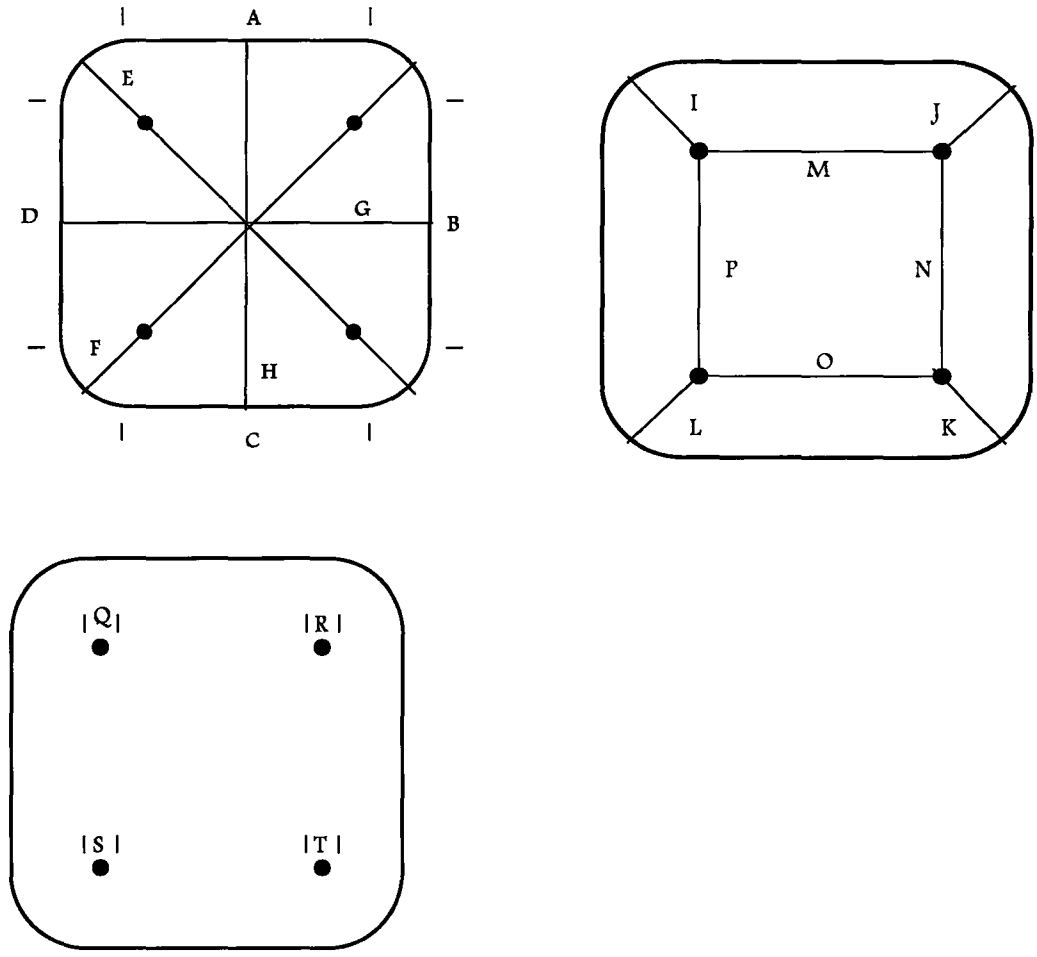

Figure 3.3: Measurements taken to assess the consistency of the thermal lesions and determine the accuracy of the model predictions. A-D are measures of the edge of the lesion, E-F the diagonal, G-H the midline, I-L the "radius". M-P are intended to be the inter-source separation, d, while Q-T are the widths of the charred regions.

4. Results and Discussion

4.1 Determining the Coagulation Radius

Figure 4.1 illustrates the results of the single fibre irradiations performed to determine the coagulation radii for a range of power-time settings.

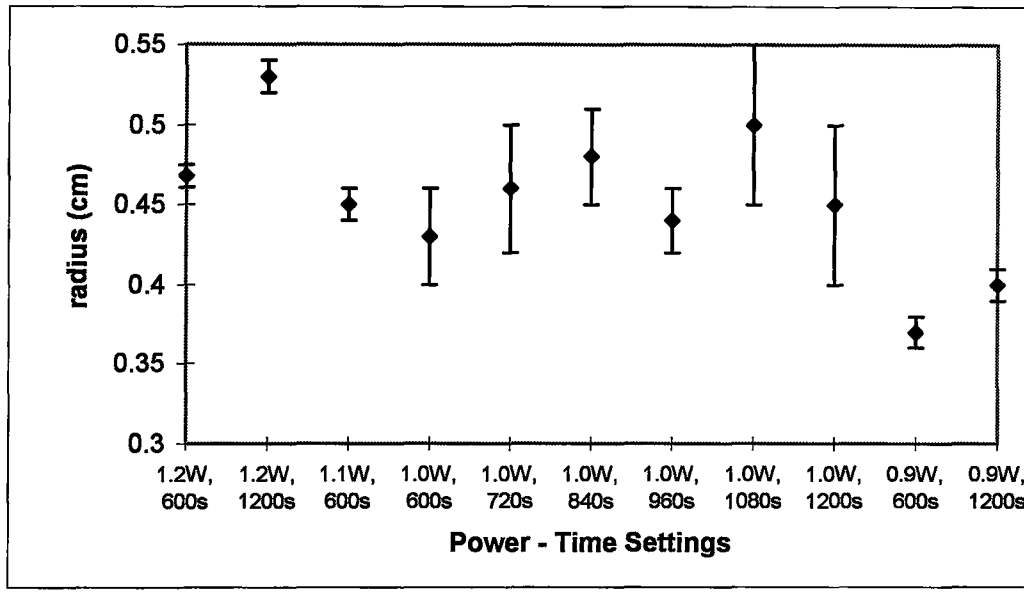

Figure 4.1: Average single source coagulation radii for a range of irradiation parameters.

Each point represents the mean radius for each setting and the error is given by the standard deviation of the mean. The magnitude of the uncertainty in each point is a reflection of the sample size at each setting.

The range of parameters tested reflects the physical limitations of the apparatus used. The lasers were operating at near maximum power to produce an output power of 1.2 W; attempting to run at any higher power for an extended period of time represented a significant risk to the lasers. Lesions smaller than that produced at 0.9 W for 600 s are not clinically relevant and would be too small for use with the multiple source delivery system.

The variation in coagulation radii over the range of irradiation settings displayed in figure 4.1 indicates that the reciprocity of delivered power and exposure duration is not valid for ILP. This means that it is not sufficient to state the total energy deposited; both the power and duration must be specified.

Typical single fibre lesions are displayed in figure 4.2. Each lesion is approximately circular in cross section and consists of an inner charred region surrounded by a white zone of coagulation. The central char is often elongated along the axis of the fibre in lesion where the exposure duration is 600s. The lesion shapes were unaffected by the presence of small vesicles (figure 4.2 D) and were only slightly distorted by larger channels (figure 4.2 G).

4.2 Steady-State Model Results

Recall that the steady-state model predicted an optimal separation of $d=3.21r_c$ and a four-source lesion dimension of $l=8.3r_c$. For 1.2 W, 600s the average coagulation radius was determined to be 0.47 ± 0.01 cm. Taking this to be an estimate of r_c, the four-source irradiations were performed with the fibres separated by 1.51 ± 0.03 cm. The results are shown in figure 4.3. The lesions produced were much smaller than predicted, poorly coalesced and did

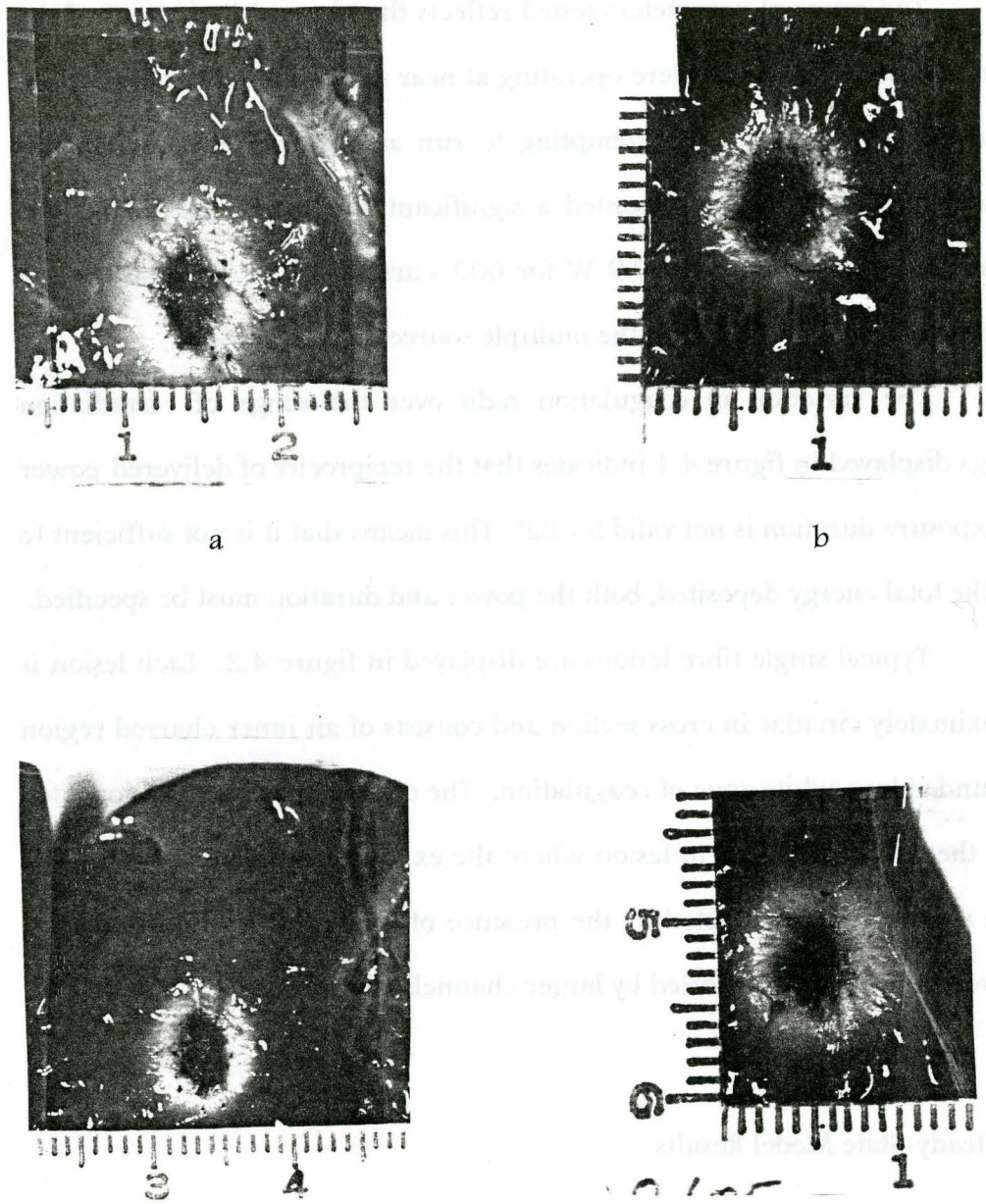

Figure 4.2: Single source lesions at (a) 1.2W, 600 s, (b) 1.2 W, 1200 s, (c) 1.1W, 600s, and (d) 1.0W, 720 s.

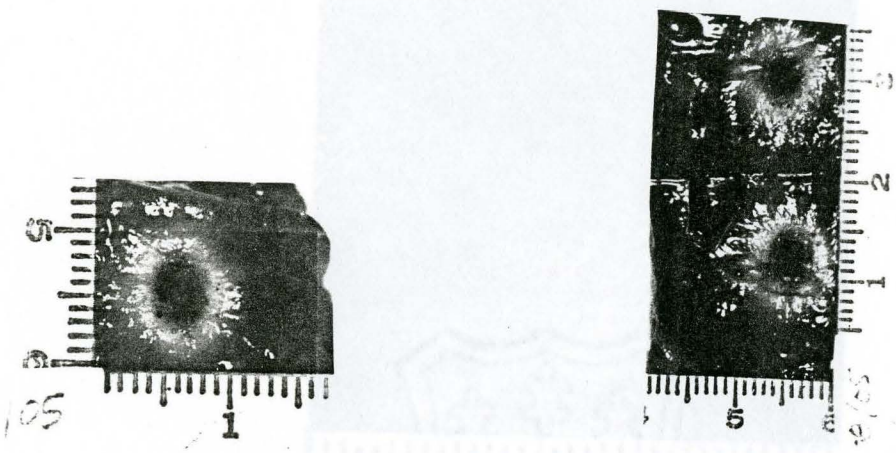

e f

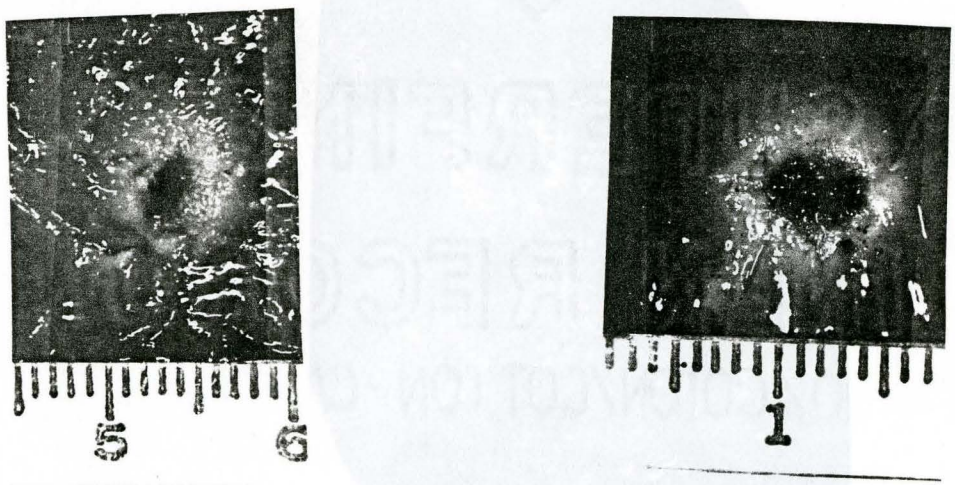

g h

Figure 4.2: Single source lesions at (e) 1.0W, 840 s, (f) 1.0 W, 1080 s, (g) 0.9W, 600s, and (h) 0.9W, 1200 s.

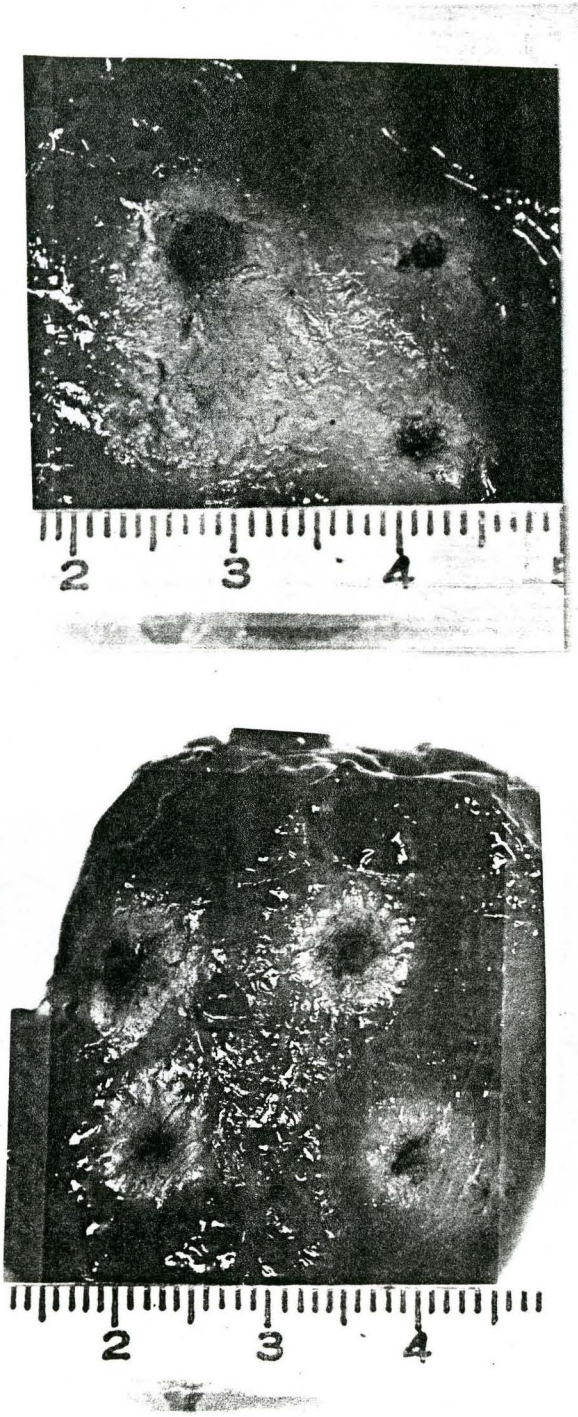

Figure 4.3: Lesions produced using $d=3.21r_c$, the optimal source separation determined by the steady-state model for 1.2W, 600s.

not match the predicted boundary shape. The discrepancies in degree of coagulation between figure 4.3 A and B are due mainly to differences in the depth of slicing through the lesion. The missing char spot in 4.3 B is also due to difficulties in slicing a non-coalescent lesion.

The fact that the lesions were smaller than predicted indicates that the temperature response must decrease more rapidly than the $1/r$ response of the steady-state model. A simulation was run using both the steady state model and the transient temperature response to determine if the sources had equilibrated by the end of 600 s.

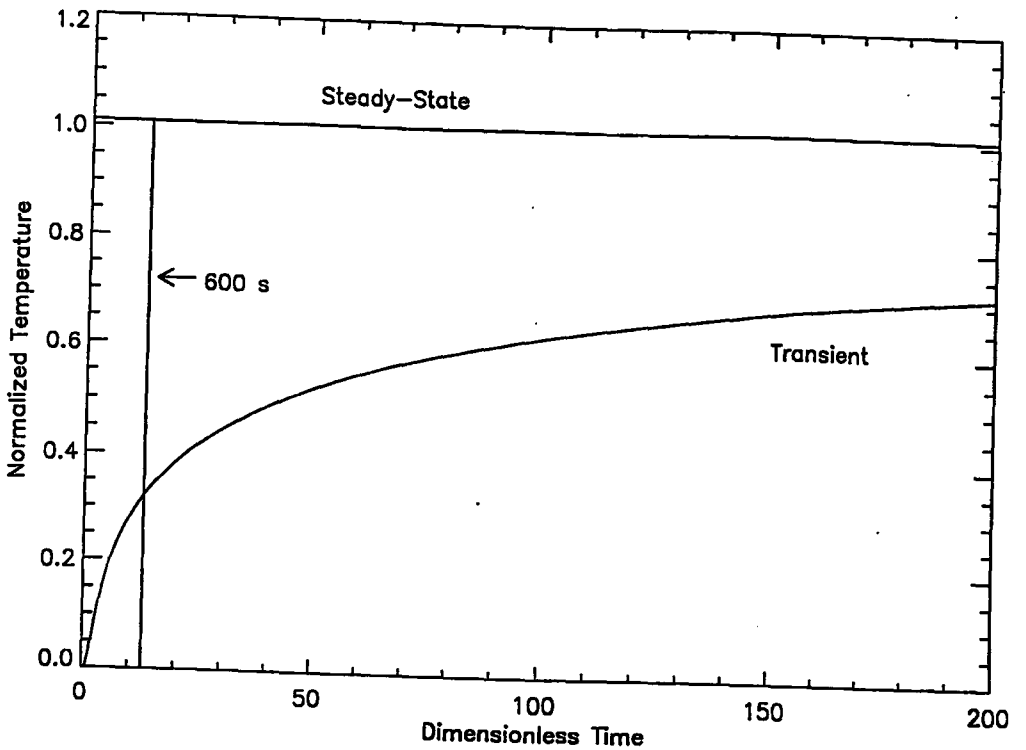

Figure 4.4: Normalised temperature increases after commencement of a four-source irradiation, illustrating the disparity between steady-state and transient temperature responses. Temperatures were calculated at a distance of r_c from one source towards a nearest neighbour source. A dimensionless time unit corresponds to 46s in this case and a temperature increase of 1 represents $P/4\pi k_{eff} r_c$.

Figure 4.4 clearly demonstrates that the steady-state temperature description overestimates the temperatures generated by the four-source array. This provided the motivation for reworking the model using transient temperature responses.

4.3 Transient Model Results

The coagulation radii determined in the first stage of experimentation were taken as approximations to $r_c(t)$ and processed through the optimising code (section 2.2) to obtain the predicted source separation and lesion size. The results are displayed in table 4.1 below.

power (W)	time (s)	dimensionless time	coagulation radius (cm)	d (cm)	w (cm)	l (cm)
1.2	600	13.1	0.47±0.01	0.97±0.01	1.25±0.02	2.22±0.02
1.2	1200	20.5	0.53±0.01	1.14±0.02	1.55±0.03	2.69±0.04
1.1	600	14.2	0.45±0.01	0.94±0.02	1.22±0.03	2.16±0.04
1.0	600	15.6	0.43±0.03	0.90±0.06	1.19±0.08	2.1±0.1
1.0	720	16.3	0.46±0.04	0.97±0.08	1.3±0.1	2.3±0.1
1.0	840	17.5	0.48±0.03	1.02±0.06	1.36±0.08	2.4±0.1
1.0	960	23.8	0.44±0.02	0.96±0.04	1.33±0.06	2.29±0.07
1.0	1080	20.7	0.50±0.05	1.1±0.1	1.5±0.1	2.6±0.1
1.0	1200	28.4	0.45±0.05	1.0±0.1	1.4±0.2	2.4±0.2
0.9	600	21.0	0.37±0.01	0.80±0.02	1.09±0.02	1.89±0.03
0.9	1200	36.0	0.40±0.01	0.91±0.02	1.30±0.03	2.21±0.04

Table 4.1: Model predictions for optimal source separations, d, and lesion size, l, based on input of measured coagulation radius and calculated dimensionless time.

The uncertainties in the coagulation radii are the standard deviations of the mean $\sigma(r_c(t))$. The uncertainties in d and w, $\sigma(d)$ and $\sigma(w)$, were determined by passing $\sigma(r_c(t))$ through the optimisation code and $\sigma(l)$ was obtained by adding $\sigma(d)$ and $\sigma(w)$ in quadrature.

Settings of 1.2 W, 600 s and 0.9 W, 600 s were chosen for four fibre testing because the $r_c(t)$ values for these were significantly different. A third setting was chosen to be 0.9 W, 1200 s because, although the $r_c(t)$ for these

parameters is significantly smaller than that at 1.2 W, 600 s, the model predicts four fibre lesions of equivalent dimensions. Typical four-source irradiation results for each setting are displayed in figure 4.5.

All lesions produced using the transient model to predict the optimal source separation were large and coalescent with smooth, convex boundaries; in other words, the lesions are clinically useful. The lesions qualitatively match the cross sectional profile displayed in figure 2.3. Figure 4.5 indicates that the shape of the lesions was generally unaffected by the presence of small vessels. An exception to this can be seen in figure 4.6 where the coagulation zone has enlarged asymmetrically around a vessel. The hole in the centre of the 0.9 W, 600 s lesion was created by the tip of the delivery cannula.

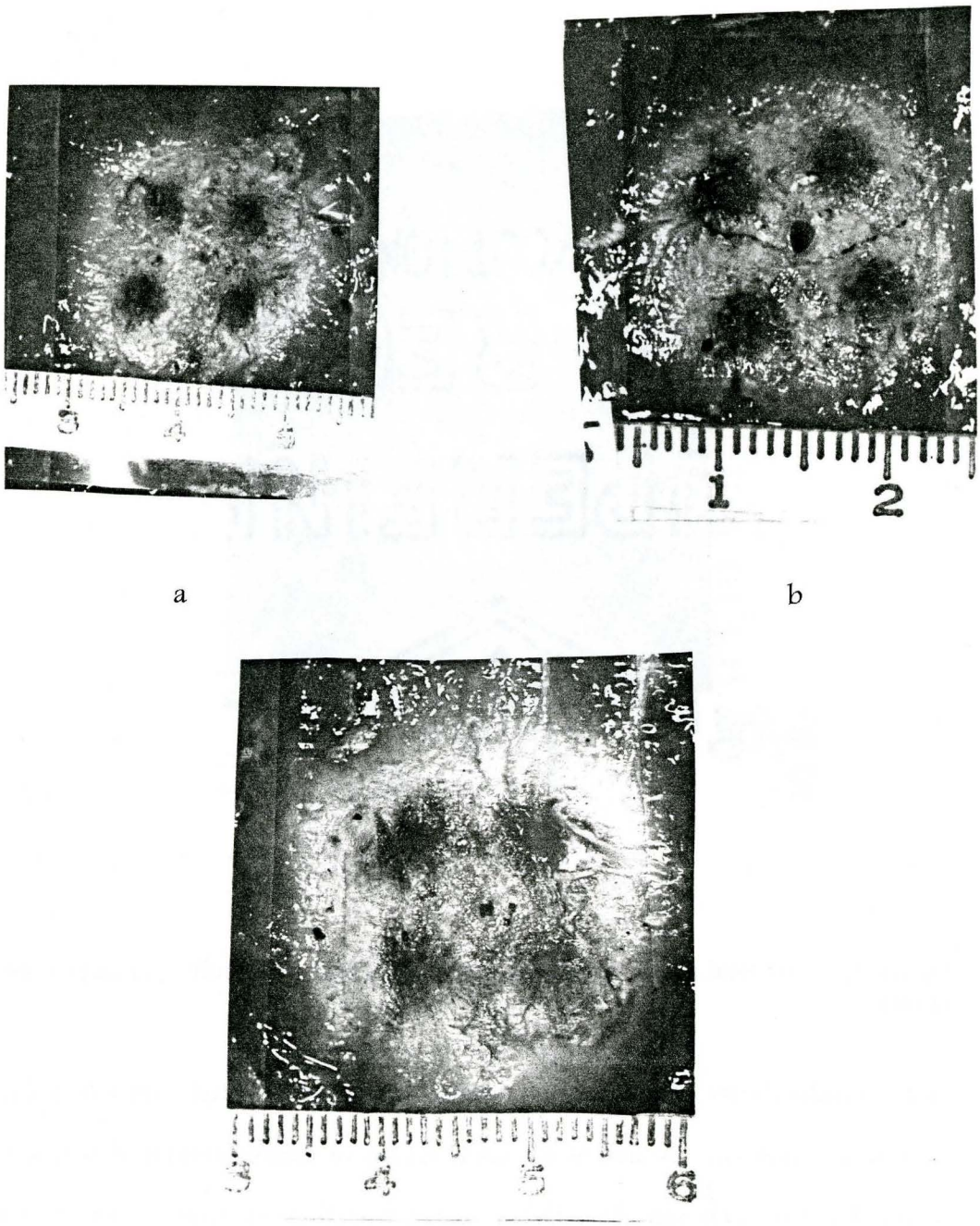

Figure 4.5: Typical lesions created using source separations predicted by the transient temperature response mathematical model (a) 1.2W, 600s, (b) 0.9W, 600s, and (c) 0.9W, 1200s

Figure 4.6: Thermal lesion produced at 0.9 W, 1200 s extending around a small vessel.

The reproducibility of the lesions created using the multiple source delivery system was assessed by averaging each group of measurements described in figure 3.3 for each sample. This average was then compared to all other samples at each irradiation setting. The results of this are displayed in figures 4.7 through 4.9. The errors displayed in these figures are the standard errors in the mean. In the cases where error bars are not visible, the uncertainties are contained within the plot symbols.

These preliminary results indicate that the coagulation volumes are reproducible. The only setting which exhibits considerable variability is 0.9W, 1200 s. Examination of figure 4.5 reveals that the extent of charring is much greater for longer exposure durations. In the 600 s lesions at both 1.2 W and 0.9 W, the charred zones are confined to four spherical regions 0.2-0.3 mm in diameter. By 1200 s these regions have become much larger as the extremely high temperature region spreads outward from the fibre tips. The char is also no longer spherical; "fingers" of carbonisation are visible between the locations of source implantations. This indicates that narrow regions of ultra-high temperature form between the sources beyond 600s of exposure. These charred volumes are very dense and consist of tissue fragments that have been fused together, consequently they are very difficult to slice through. The resulting inconsistencies are the probable cause of the inter-sample variability at this setting.

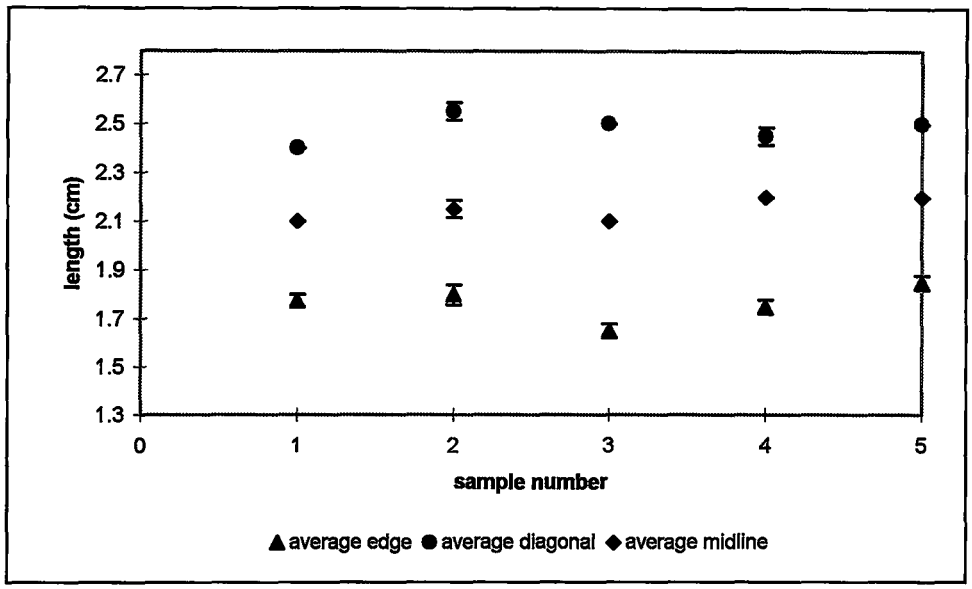

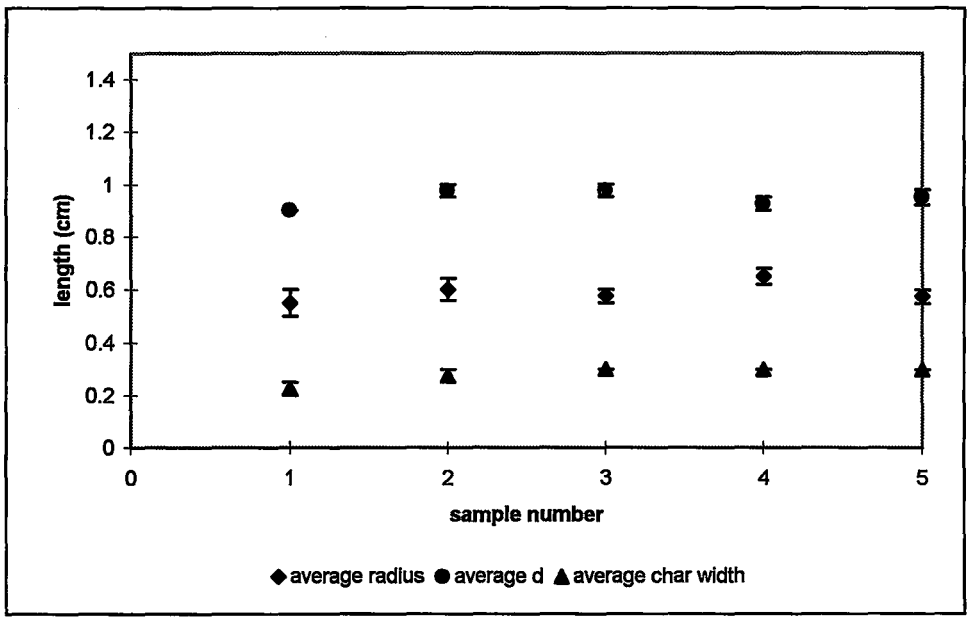

Figure 4.7: Reproducibility of lesions created using the multiple fibre delivery system for a setting of 1.2 W, 600 s lesions.

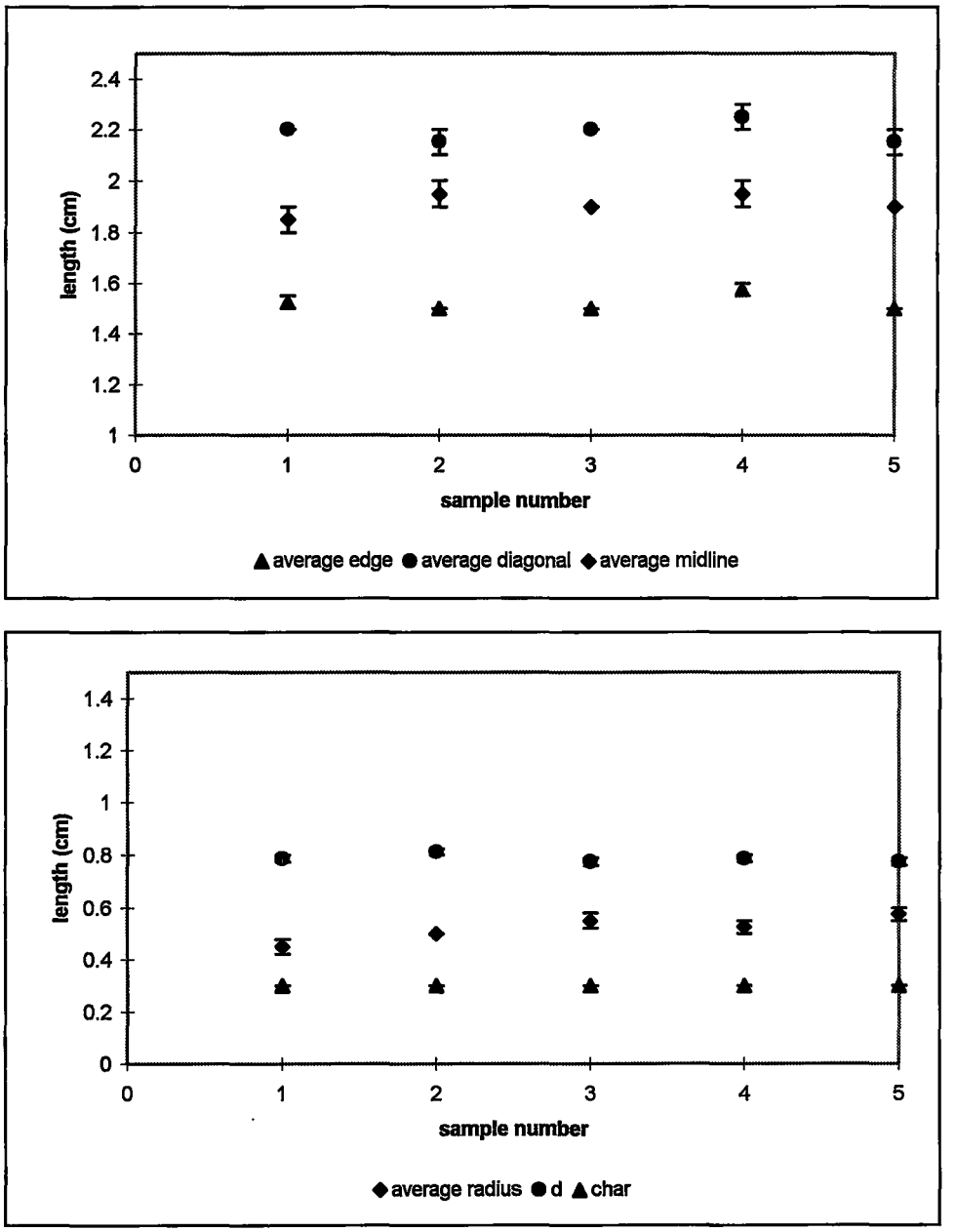

Figure 4.8: Reproducibility of lesions created using the multiple fibre delivery system for a setting of0.9 W, 600 s lesions

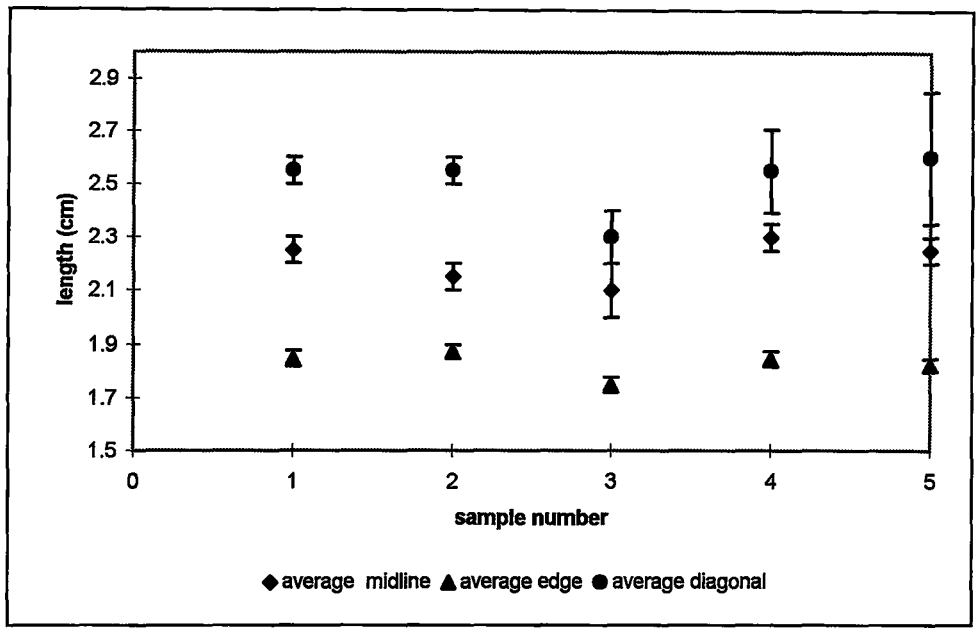

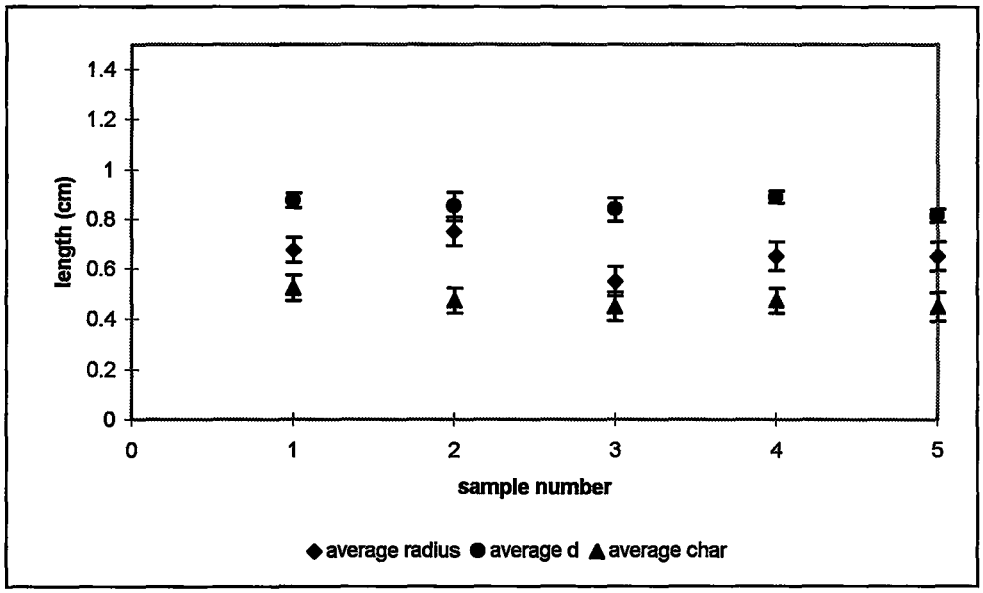

Figure 4.9: Reproducibility of lesions created using the multiple fibre delivery system for a setting of 0.9 W, 1200 s.

The midline measures from each sample were averaged to obtain the experimental lesion size for each irradiation setting. Figure 4.10 demonstrates that the transient temperature model, equation 2.20, provides an accurate prediction of the lesion dimensions. Accuracy of fibre placement was determined by comparing the average measured separation of the centres of the char spots to the distance set by the model. The results of this comparison can be seen in figure 4.11. The discrepancy at 0.9 W, 1200 s is the result of a systematic measuring error. The large regions of char present in these lesions caused difficulty in determining the separations of the centres resulting in a consistent under estimation of d.

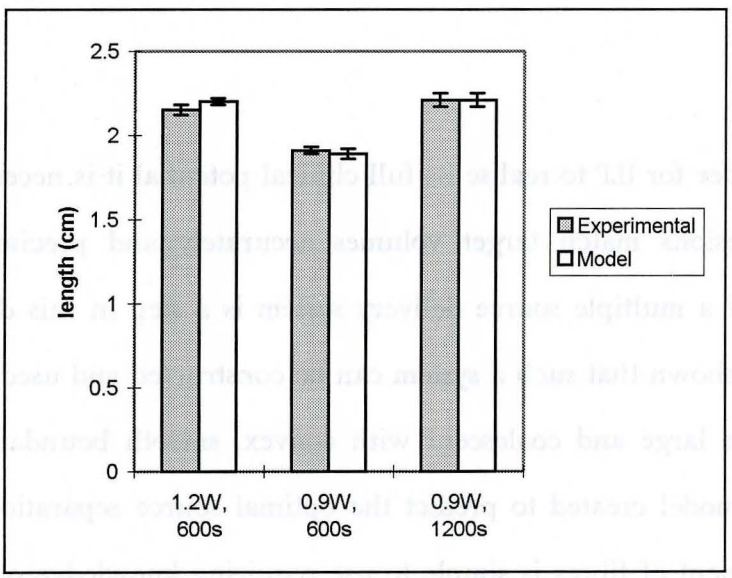

Figure 4.10: Comparison of experimental lesion dimensions with model predictions for three sets of irradiation parameters.

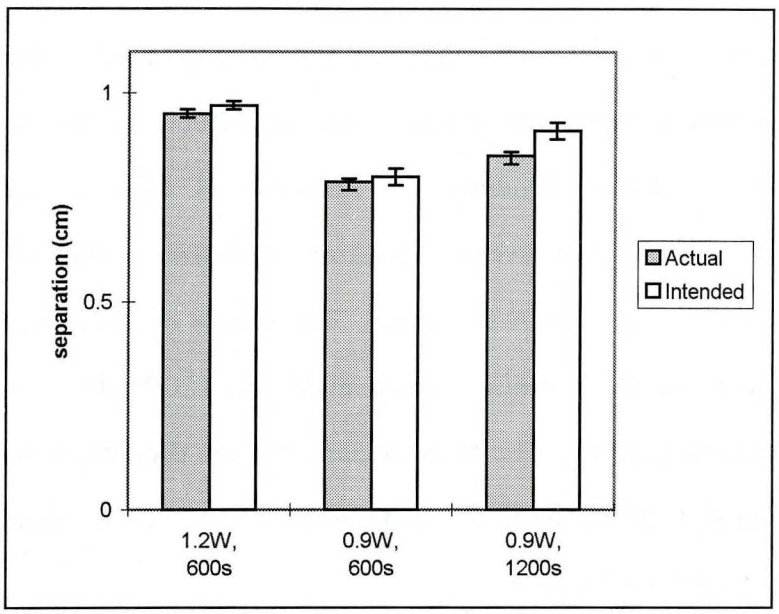

Figure 4.11: Comparison of actual and intended source separations for each of the test settings.

4.4 Summary

In order for ILP to realise its full clinical potential it is necessary that the thermal lesions match target volumes accurately and precisely. The development of a multiple source delivery system is a step in this direction. This work has shown that such a system can be constructed and used to create lesions that are large and coalescent with convex, smooth boundaries. The mathematical model created to predict the optimal source separation for the given arrangement of fibres is simple to use requiring knowledge of only the exposure duration and the single source coagulation radius. Figure 4.10 clearly demonstrates that the model provides an accurate prediction of lesion dimensions.

The principle limitations of the model are that it applies to a single arrangement of fibres and that it does not consider perfusion cooling or the spatiotemporal variations of tissue parameters. It does, however, demonstrate that it is possible to predict the shape of a multiple fibre lesion, at least within the plane defined by the sources. A further assessment of the model's ability to predict the thickness of the lesion would aid in determining the distance one would be able to retract the fibres in order to re-irradiate without leaving cold-spots within the tumour.

The multiple source delivery system is simple to use. Preparation for *ex vivo* irradiation, consisting of rough polishing the application fibre end, marking the extension distance on each fibre and inserting the fibres into the cannula can be completed in ten minutes. For *in vivo* use preparation time will necessarily be extended but will always be less than for individual fibre insertion. A further advantage of the multiple source cannula over current modes of multiple fibre irradiation is that it can produce lesions with varying source separation with a single cannula and even through a single incision.

Future work in this area should extend the mathematical model and experiments to *in vivo* situations and make it fully three-dimensional. Another stage of development should be to solve the inverse problem of determining the optimal arrangement of fibres required to treat a given arbitrary volume. This would become the foundation for customised treatment planning for ILP, enhancing its clinical viability.

Bibliography

Agah R., Pearce J.A., Welch A.J., *et al.*, 1994 "Rate process model for arterial tissue thermal damage: Implications on vessel photocoagulation" Lasers Surg. Med. 15 p.176.

Amin Z., Bown S.G., and Lees W.R., 1993 "Liver tumour ablation by interstitial laser photocoagulation: Review of experimental and clinical studies" Intervent. Radiol. 10 p.88.

Amin Z., Buonaccorsi G., Mills T., *et al.*, 1993 "Interstitial laser photocoagulation: Evaluation of a 1320 nm Nd-YAG and an 805 nm diode laser: The significance of charring and the value of pre-charring the fibre tip" Lasers Med. Sci. 8 p.113.

Amin Z., Donald J., Masters A., *et al.*, 1993 "Hepatic metastases: Interstitial laser photocoagulation with real-time US monitoring and dynamic CT evaluation of treatment" Radiology 187 p.339.

Arkin H., Xu L.X., and Holmes K.R., 1994 "Recent developments in modelling heat transfer in blood perfused tissues" IEEE Trans. Biomed. Eng. 41 p.97

Beacco C.M., Mordon S.R., and Brunetaud J.M., 1994 "Development and experimental in vivo validation of mathematical modelling of laser coagulation" Lasers Surg. Med. 14 p.362.

Birngruber R., "Thermal modelling in biological tissues", in Lasers in Biology and Medicine, ed. by Hillenkamp F., Pratesi R., and Sacchi C.A. Plenum Press, New York, 1980.

Bleier A.R., Jolesz F.A., Cohen M.S., *et al.*, 1991 "Real-time magnetic resonance imaging of laser heat deposition in tissue" Magn. Reson. Med. 21 p.132.

Bown S.G., 1983 "Phototherapy of tumours" World J. Surg. 7 p.700.

Breasted J.H., The Edwin Smith Surgical Papyrus, vol. 1, University of Chicago Press, Chicago, 1930.

Brinck H. and Werner J., 1994 "Efficiency function: Improvement of classical bioheat approach" J. Appl. Physiol. 77 p.1617.

Busch W., 1866 "Uber den Einfluss weichen Hefitigere Erysipelen Zuweilen auf Organisierte Neubildungen Ausuken Verhandl" Rheinisch-Westfal. Akad. Wiss. Nat. Ing. Wirtschaftswiss 23 p.28.

Carslaw H.S. and Jaeger J.C., Conduction of Heat in Solids, 2nd ed., Oxford University, New York, 1989.

Castro D.J., Lufkin R.B., Saxton R.E., *et al.*, 1992 "MRI and/or US guided interstitial Nd:YAG laser phototherapy for palliative treatment of recurrent head and neck tumours: Clinical experience" Lasers Surg. Med. Suppl. 4 p.48.

Coley W.B., 1893 "The treatment of malignant tumours by repeated inoculations of erysipelas: with a report of ten original cases" Am. J. Med. Sci. 105 p.487.

Dachman A.H., McGehee J.A., Beam T.E., *et al.*, 1990 "US-guided percutaneous laser ablation of liver tissue in a chronic pig model" Radiology 176 p.129.

Davis M., Dowden J., Steger A., *et al.*, 1988 "A mathematical model for interstitial laser treatment of tumours using four fibres" Laser Med. Sci. 41 p.41.

Dowden J., Jordan T., Kapadia P., 1988 "Temperature distribution produced by a cylindrical etched fibre tip in laser treatment of tumours by local hyperthermia" Lasers Med. Sci. 3 p.47.

Dowlatshahi K., Bhattacharya A.K., Silver B., *et al.*, 1991 "Percutaneous interstitial laser therapy of a patient with recurrent hepatoma in a transplanted liver" Surgery 112 p.603.

Dowlatshahi K., Babish D., Bangert J.D., Kluiber, R., 1992 "Histologic evaluation of rat mammary tumour necrosis by interstitial Nd:YAG laser hyperthermia" Lasers Surg. Med. 12 p.159.

Frank F., 1989 "Laser light and tissue: Biophysical aspects of medical laser application" SPIE (Lasers and Medicine) 1353 p.37.

Hahl J., Haapiainen R., Ovaska J., *et al.*, 1990 "Laser-induced hyperthermia in the treatment of liver tumours" Lasers Surg. Med. 10 p.319.

Hall E.J., Radiobiology for the Radiologist, 3rd ed., Lippencott, Philadelphia, 1988.

Harries S.A., Amin Z., Smith E.F., *et al.*, 1994 "Interstitial laser photocoagulation as a treatment for breast cancer" Br. J. Surg. 81 p.1617.

Hillenkamp F., "Interaction between laser radiation and biological systems", in Lasers in Biology and Medicine, ed. Hillenkamp F., Pratesi R., and Sacchi C.A., Plenum Press, New York, 1980.

Hu C-L. and Barnes F.S., 1970 "The thermal-chemical damage in biological material under laser irradiation" IEEE Trans. Biomed. Eng. BME-17 p.220.

Jacques S.L. and Prahl S.A., 1987 "Modelling optical and thermal distributions in tissue during laser irradiation" Lasers Surg. Med. 6 p.494.

Jacques S.L., Rastegar S., Motamedi M., *et al.* "Liver photocoagulation with diode laser (805 nm) vs. Nd:YAG laser (1064 nm)", in SPIE Proceedings, Laser-Tissue Interaction III, vol. 1646, Los Angeles, 1992.

Malone D.E., Lesiuk L., Brady A.P., *et al.*, "Intravascular gas production during hepatic interstitial laser photocoagulation (ILP): Non-invasive demonstration and possible clinical significance" Radiology (in press).

Malone D.E., Wyman D.R., DeNardi F.G., *et al.*, 1994 "Hepatic interstitial laser photocoagulation: An investigation of the relation ship between acute thermal lesions and their sonographic images" Invest. Radiol. 29 p.915.

Malone D.E., Wyman D.R., DeNardi F.G., *et al.*, 1992 "Sonagraphic changes during hepatic interstitial laser photocoagulation: An investigation of three optical fibre tips" Invest. Radiol. 27 p.804.

Masters A., Steger A.C., and Bown S.G., 1991 "Role of interstitial therapy in the treatment of liver cancer" Br. J. Surg. 78 p.518.

Matthewson K., Barr H., Tralau C., and Bown S.G., 1989 "Low power interstitial Nd:YAG laser photocoagulation: Studies in a transplantable fibrosarcoma" Br. J. Surg. 76 p.378.

McKenzie A.L., 1990 "Physics of thermal processes in laser-tissue interaction" Phys. Med. Biol. 35 p.1175.

Nolsøe C.P., Torp-Pedersen S., Burcharth F., *et al.*, 1993 "Interstitial hyperthermia of colorectal liver metastases with a US-guided Nd-YAG laser with a diffuser tip: A pilot clinical study" Radiology 187 p.333.

Nolsøe C.P., Torp-Pedersen S., Olldag E., *et al.*, 1992 "Bare fibre low power Nd-YAG laser interstitial hyperthermia: Comparison between diffuser tip and non-modified tip: An in vitro study" Lasers Med. Sci. 7 p.1.

Ohyama M., Nobori T., Moriama I., *et al.*, 1988 "Laserthermia on head and neck malignancies: Experimental and clinical studies" Acta Otolaryngol. Suppl. 4 p.48.

Panjehpour M., Overholt B.F., Milligan A.J., *et al.*, 1990 "Nd:YAG laser-induced interstitial hyperthermia using a long frosted contact probe" Lasers Surg. Med. 10 p.16.

Pearce J.A., "Thermodynamic principles of laser-tissue interaction", in Annual International Conference of the IEEE Engineering in Medicine and Biology Society Proceedings, vol. 12, 1990.

Pearce J.A. and Thomsen S., "Kinetic models of laser-tissue fusion processes", ISA paper #93-044, 1993.

Prapavat V., Roggan A., Walter J., *et al.*, 1996 "In vitro studies and computer simulations to assess the use of a diode laser (805 nm) for laser induced thermotherapy (LITT)" Lasers Surg. Med. 18 p.22.

Raven P.H. and Johnson G.B., Biology, p.70, Times Mirror/Mosby College Publishing, Toronto, 1986

Roux F.X., Merienne L., Leriche B., *et al.*, 1992 "Laser interstitial thermotherapy in stereotactical neurosurgery" Laser Med. Sci. 7 p.121.

Schatz S.W., Bown S.G., Wyman D.R., *et al.*, 1992 "Low power interstitial Nd-YAG laser photocoagulation in normal rabbit brain" Lasers Med. Sci. 7 p.433.

Schrottner O., Ascher P.W., and Ebner F., "Interstitial laser thermotherapy of brain tumours under MRI control", Abstract C-24, p.66, in Fifith International Congress of the European Laser Association, Graz, Austria, 1990.

Steger A.C., Lees W.R., Shorvon P., *et al.*, 1992 "Multiple-fibre low-power interstitial laser hyperthermia: Studies in normal liver" Br. J. Surg. 79 p.139.

Steger A.C., Lees W.R., Walmsley K., and Bown S.G., 1989 "Interstitial laser hyperthermia: A new approach to local destruction of tumours" Br. Med. J. 299 p.362.

Steger A.C., Shorvon P., Walmsley K., *et al.*, 1992 "Ultrasound features of low power interstitial laser hyperthermia" Clin. Radiol. 46 p.88.

Svaasand L.O., Boerslid T., and Oeveraasen M., 1985 "Thermal and optical properties of living tissue: Application to laser-induced hyperthermia" Lasers Surg. Med. 5 p.589.

Svaasand L.O., 1989 "Dosimetry for laser induced hyperthermia" Laser Med. Sci. 4 p.309.

Svaasand L.O., Gomer C.J., and Morinelli E., 1990 "On the physical rationale of laser induced hyperthermia" Lasers Med. Sci. 5 p.121.

Thomsen S., 1990 "Pathologic analysis of photothermal and photochemical effects of laser-tissue interactions" Photochem. Photobiol. 53 p.825.

van Hillegersberg R., van Staveren H.J., Roggan A., *et al.*, 1995 "Interstitial laser photocoagulation as a treatment for breast cancer" Correspondence, Br. J. Surg. 82 p.856.

van Hillegersberg R., van Staveren H.J., Kort W.J., *et al.*, 1994 "Interstitial Nd:YAG laser coagulation with a cylindrical diffusing fibre tip in experimental liver metastases" Lasers Surg. Med. 14 p.124.

Vyas R. and Rustgi M.L., 1992 "Green's function solution to the tissue bioheat equation" Med. Phys. 19 p.1319.

Weinbaum S. and Jiji L.M., 1985 "A new simplified bioheat equation for the effect of blood flow on local average tissue temperature" J. Biomech. Eng. 107 p.131.

Welch A.J., 1984 "The thermal response of laser irradiated tissue" IEEE J. Quantum Electron. QE-20 p.1471.

Whelan W.M., Wyman D.R., Wilson B.C., 1995 "Investigations of large vessel cooling during interstitial laser heating" Med. Phys. 22 p.105.

Wilson B.C., "Modelling and measurements of light propagation in tissue for diagnostic and therapeutic applications", in Laser systems for Photobiology and Photomedicine, ed. Chester A.N. *et al.*, Plenum Press New York, 1991.

Wyman D.R., 1993 "Selecting source locations in multifibre interstitial laser photocoagulation" Lasers Surg. Med. 13 p.656.

Wyman D.R., Schatz S.W., and Maguire J.A.C., "A comparison of 810 nm and 1064 nm wavelengths for interstitial laser photocoagulation in rabbit brain" Invest. Radiol. (in press)

Wyman D.R. and Whelan W.M., 1994 "Basic optothermal diffusion theory for interstitial laser photocoagulation" Med. Phys. 21 p.1651.

Wyman D.R., Whelan W.M., and Wilson B.C., 1992 "Interstitial laser photocoagulation: Nd:YAG 1064 nm optical fibre source compared to

a point heat source" Lasers Surg. Med. 12 p.659.

Wyman D.R., Wilson B.C., and Adams K., 1994 "Dependence of laser photocoagulation on interstitial delivery parameters" Lasers Surg. Med. 14 p.59.

Yoon G., Welch A.J., Motamedi M., and van Gemert M.C.J., 1987 "Development and application of three-dimensional light distribution model for laser irradiated tissue" IEEE J. Quantum Electron. QE-23 p.1721.

Appendix

Program One: Determining the lesion boundary

```
; This is the function used to calculate the boundary for the steady-state case

function foursc1,z
common boundary,x,y,rc

; dis is the inter-source separation, rc is the coagulation radius, x, y, and z are
; the  usual Cartesian co-ordinates

  dis=3.21*rc
  a=x^2+y^2+z^2+dis^2/2*rc^2
  b=(a-dis*sqrt(2)*x*rc)^0.5
  c=(a+dis*sqrt(2)*x*rc)^0.5
  d=(a-dis*sqrt(2)*y*rc)^0.5
  e=(a+dis*sqrt(2)*y*rc)^0.5

  return, [(rc/b)+(rc/c)+(rc/d)+(rc/e)-1]


end

; This is the function used to determine the boundary for the transient case

function foursc2,z
common boundary,x,y,rc

; time is the time in s,  tau is the dimensionless time

  time=600
  dis=2.08*rc
  tau=time*(4.8e-3)/rc^2
  rttau=sqrt(tau)
  denom=rc*rttau

  sq=x^2+y^2+z^2+(dis^2*rc^2)/2
  a=(sq-dis*sqrt(2)*x*rc)^(0.5)
  b=(sq+dis*sqrt(2)*x*rc)^(0.5)
  c=(sq-dis*sqrt(2)*y*rc)^(0.5)
  d=(sq+dis*sqrt(2)*y*rc)^(0.5)
  e=1-errorf(a/denom)
  f=1-errorf(b/denom)
```

```
  g=1-errorf(c/denom)
  h=1-errorf(d/denom)
  i=1-errorf(1/rttau)

  return, [(e/a)+(f/b)+(g/c)+(h/d)-(i/rc)]

end

; THIS IS THE MAIN PROGRAM:
; THIS IS A PROGRAM TO DETERMINE THE SHAPE OF THE LESION
; BOUNDARY DUE TO 4 COPLANAR SOURCES

pro canulla

; DEFINE A BLOCK COMMON TO THE FUNCTION


common boundary,x,y,rc

; DEFINE THE MAGNITUDE OF THE COAGULATION RADIUS IN CENTIMETRES


rc=0.47

; DEFINE AN ARRAY TO STORE THE ROOTS AS THEY ARE DETERMINED


rt=fltarr(30,30)
xax=fltarr(30)
yax=fltarr(30)

; SET THE STEP SIZE, CHOSEN SO THAT THE LESION FILLS THE GRAPH PLANE

inc =1.5/30

; INITIAL Z GUESS

z=findgen(1000)/999 * 5

; ENSURE THAT ALL DEVICES ARE CLOSED

close,/all

; OPEN FILES TO WRITE RESULTS TO

openw, 1, 'rootx.dat'
openw, 2, 'rooty.dat'
openw, 3, 'rootz.dat'
```

```
; SET X AND Y TO ZERO AND STEP THROUGH THE PLANE DETERMINING THE
; ROOTS.

 x=0
 for i=0,29 do begin
    y=0
;   print,i
    for j=0,29 do begin

       tmp = foursc2(z)
       k=where(tmp gt 0)
       l=z((n_elements(k)-1))

      please=foursc2(0)
      please=please(0)

        if ( please ge 0.0) then begin
        rt(i,j)=nr_newt(l,'foursc2',itmax=15,/double)
        printf,1,x
        printf,2,y
        printf,3,rt(i,j)
        endif

    y=y+inc
  endfor
  x=x+inc
 endfor

close,/all

; SO FAR WE ONLY HAVE ONE QUADRANT OF THE LESION SO WE NEED TO
; COPY THE ROOTS INTO THE OTHER THREE QUADRANTS TO GET A FULL
; LESION

final=fltarr(60,60)
final(30:*,30:*)=rt
final(30:*,0:29)=rotate(rt,3)
final(0:29,*)=rotate(final(30:*,*),2)

; THIS CREATES A COORDINATE AXIS AS OPPOSED TO AN ARRAY UNIT AXIS

xax=findgen(60)/59*3
yax=findgen(60)/59*3

;THESE COMMANDS CREATES A SURFACE PLOT OF THE LESION

surface, final, xtitle=' (cm)', ytitle=' (cm)', ztitle='(cm)' , zrange=[0,5]

end
```

Program Two: Optimising the source separation for the transient temperature response model

```
; This is the temperature reponse to be optimised

function optimal,x
common op,tau,rc

; rc is the coagulation radius, x(0) is d, x(1) is w, tau is the dimensionless time

a = 2/sqrt(!pi)
b = (x(0)/2)^2 + (x(1)/2)^2
d = (x(1)/2 + x(0))
c = (x(0)/2)^2 + d^2
e = rc*sqrt(tau)
f=-A*exp(-(b/e^2))*(b^(-1)/(4*e))*(x(1)-x(0))
g=(1-errorf(b^(0.5)/e))*((b^(-1.5))/4)*(x(0)-x(1))
h=-A*exp(-(c/e^2))*(c^(-1)/e)*(-d/2-x(0)/4)
i=(1-errorf(c^(0.5)/e))*(c^(-1.5))*(d/2+x(0)/4)
j=(1-errorf(b^(0.5)/e))*rc*b^(-0.5)
k=(1-errorf(c^(0.5)/e))*rc*c^(-0.5)
l=(1-errorf(1/sqrt(tau)))/2
m=f+g+h+i
n=j+k-l

return,[m,n]

end

; This is the function to determine the error in d and w based on the error in rc

function opterr,x
common oper,taur,er

a = 2/sqrt(!pi)
b = (x(0)/2)^2 + (x(1)/2)^2
d = (x(1)/2 + x(0))
c = (x(0)/2)^2 + d^2
e = er*sqrt(taur)
f=-A*exp(-(b/e^2))*(b^(-1)/(4*e))*(x(1)-x(0))
g=(1-errorf(b^(0.5)/e))*((b^(-1.5))/4)*(x(0)-x(1))
h=-A*exp(-(c/e^2))*(c^(-1)/e)*(-d/2-x(0)/4)
 i=(1-errorf(c^(0.5)/e))*(c^(-1.5))*(d/2+x(0)/4)
 j=(1-errorf(b^(0.5)/e))*er*b^(-0.5)
 k=(1-errorf(c^(0.5)/e))*er*c^(-0.5)
  l=(1-errorf(1/sqrt(taur)))/2
 m=f+g+h+i
  n=j+k-l
  return,[m,n]
```

```
end

; THIS IS THE MAIN PROGRAM USED TO CALCULATE THE OPTIMAL D AND W
; FOR A GIVEN RC.

pro transopt
common op,tau,rc
common oper,taur,er

;RC IS THE COAGULATION RADIUS, TIME IS THE EXPOSURE DURATION, TAU
;THE DIMENSIONLESS TIME, TAUR IS THE SAME THING 'CAUSE YOU CAN'T
; HAVE THE SAME VARIABLE IN TWO COMMON BLOCKS

rc=0.4
time=1200
tau=(4.8e-3)*time/rc^2
print,'tau=',tau
taur=(4.8e-3)*time/rc^2
print,'taur=',taur

; THIS WILL ALSO DETERMINE THE ERROR IN D AND W USING THE ERROR IN
; RC, ER

er=0.01

; X IS THE GUESS FOR D AND W, Y IS THE GUESS FOR THE ERRORS

x=[1,1]
y=[0.01,0.01]

res=nr_newt(x,'optimal',/double)
erres=nr_newt(y,'opterr',/double)

; PRINT OUT THE RESULTS

print,'d is ',res(0)
print,'err(d) is', erres(0)
print,'w is ',res(1)
print,'err(w) is', erres(1)

end
```

Program Three: Determining the transient temperature profile

```
pro tprofile
```

```
;THIS IS A PROGRAM FOR CALCULATING AND PLOTTING TEMPERATURE
;PROFILES FOR ANY GIVEN SOURCE-SOURCE DISTANCES.
;THE PROFILES ARE FOR ALL DIMENSIONLESS TIME AT A POINT THAT IS ONE
;COAGULATION RADIUS AWAY FROM A SOURCE, TOWARDS A NEAREST
;NEIGHBOUR SOURCE.
;ALL DISTANCES ARE IN CM.

; RC IS THE COAGULATION RADIUS, DS IS THE SOURCE SEPARATION, TAU
;IS THE DIMENSIONLESS TIME

rc=0.47
ds=0.97
time=findgen(10000)+1
tau=(4.83e-3*time)/rc^2

;D IS THE DISTANCE FROM THE ORIGIN TO THE SOURCE IN QUESTION

D=ds/sqrt(2)

;O IS THE LENGTH OF THE OPPOSITE SIDE OF THE TRIANGLE, A THAT OF THE
;ADJACENT

O=ds/2
A=O

;R IS THE LENGTH OF THE VECTOR TO THE FIELD POINT

q=O-rc
r=sqrt(q^2+A^2)

;THETA IS THE ANGLE TO THE FIELD POINT

theta=atan(q/A)

; CALCULATING T WHICH IS THE TEMPERATURE PROFILE

dis=r-D
ang1=theta-(!pi/4)
ang2=theta-((3*!pi)/4)
ang3=theta-((5*!pi)/4)
ang4=theta-((7*!pi)/4)

denom=rc*sqrt(tau)

top1=(sqrt(dis^2+ang1^2))
top2=(sqrt(dis^2+ang2^2))
top3=(sqrt(dis^2+ang3^2))
top4=(sqrt(dis^2+ang4^2))
```

```
erf1=1-errorf(top1/denom)
erf2=1-errorf(top2/denom)
erf3=1-errorf(top3/denom)
erf4=1-errorf(top4/denom)

bott1=top1/rc
bott2=top2/rc
bott3=top3/rc
bott4=top4/rc

T=erf1/bott1+erf2/bott2+erf3/bott3+erf4/bott4

; CALCULATE THE STEADY-STATE TEMPERATURE AT THE SAME POINT

Tsteady=1/bott1+1/bott2+1/bott3+1/bott4

print,Tsteady

; PLOT THE PROFILES

set_plot,'ps'
plot,tau,T,yrange=[0,1.2],xrange=[0,200],xtitle='Dimensionless Time', $
ytitle='Normalized Temperature'
plots,[0,200],[Tsteady,Tsteady]
xyouts,150,0.6,'Transient'
xyouts,50,1.05,'Steady-State'
plots,[13,13],[0,Tsteady]
xyouts,25,0.7,'600 s'
arrow,23,0.72,15,0.72,/data
device,/close

end
```